International Journal of Modern Physics D
© World Scientific Publishing Company

arXiv:astro-ph/0410182v1 7 Oct 2004

MAGNETIC FIELDS IN CLUSTERS OF GALAXIES

FEDERICA GOVONI
Dipartimento di Astronomia, Universitá di Bologna, Via Ranzani 1, I-40127 Bologna, Italy
fgovoni@ira.cnr.it

LUIGINA FERETTI
Istituto di Radioastronomia CNR/INAF, Via Gobetti 101, I-40129 Bologna, Italy
lferetti@ira.cnr.it

Received (Day Month Year)
Revised (Day Month Year)

The existence of magnetic fields associated with the intracluster medium in clusters of galaxies is now well established through different methods of analysis. Magnetic fields are investigated in the radio band from studies of the rotation measure of polarized radio galaxies and the synchrotron emission of cluster-wide diffuse sources. Other techniques include X-ray studies of the inverse Compton emission and of cold fronts and magneto hydrodynamic simulations. We review the main issues that have led to our knowledge on magnetic fields in clusters of galaxies. Observations show that cluster fields are at the μG level, with values up to tens of μG at the center of cooling core clusters. Estimates obtained from different observational approaches may differ by about an order of magnitude. However, the discrepancy may be alleviated by considering that the magnetic field is not constant through the cluster, and shows a complex structure. In particular, the magnetic field intensity declines with the cluster radius with a rough dependence on the thermal gas density. Moreover, cluster magnetic fields are likely to fluctuate over a wide range of spatial scales with values from a few kpc up to hundreds kpc. Important information on the cluster field are obtained by comparing the observational results with the prediction from numerical simulations. The origin of cluster magnetic fields is still debated. They might originate in the early Universe, either before or after the recombination, or they could have been deposited in the intracluster medium by normal galaxies, starburst galaxies, or AGN. In either case, magnetic fields undergo significant amplification during the cluster merger processes.

Keywords: Clusters of galaxies; Magnetic field; Intracluster medium; Radio emission; Non-thermal emission

1. Introduction

Experience indicates that most of the matter in the Universe is composed of ionized or partially ionized gas permeated by magnetic fields. Celestial objects are magnetized and magnetic fields of significant strength are found everywhere in the interstellar space, and over small and very large scales, in the extragalactic universe.

In general, small compact objects have the largest magnetic field strengths, while larger low-density objects have weaker magnetic fields.

The Earth has a bipolar field of about 0.5 G at its surface, originating from an idealized current due to the charged fluid motion going circularly in a ring inside the liquid molten metallic core. On the Jupiter surface the magnetic field is about 4 G, owing to the fast Jupiter rotation. In the interplanetary space of the solar system the magnetic fields are of the order of 50 μG.

On the Sun, the magnetic field is of 10 G at the poles, while localized sunspots on the surface near the equatorial zone of the Sun, and more generally of a star, can have magnetic field strengths of 2000 G. In protostellar envelopes and protostars, fields are of $\sim$ 1 mG. A bipolar field is "frozen" into the gas of a star during the contraction from a normal star to a degenerate star. It will remain bipolar-shaped but its intensity will increase as r^{-2}, thus magnetic fields of pulsars and neutron stars are of the order of 10^{12} G, those of white dwarfs are around 10^6 G.

A widespread field of $\sim$ 5 μG, characterized by a spiral shape, is present in the Galaxy. At the Galaxy nucleus, highly organized filaments with strength of $\sim$ 1 mG are detected. Fields in other spiral galaxies are of $\sim$ 10 μG on average, with values up to $\sim$ 50 μG in starburst galaxies and $\sim$ 30 μG in massive spiral arms.

Fields of $\sim$ μG are found in the radio emitting lobes of radio galaxies. Fields of similar or weaker strength are detected in the intracluster medium of clusters of galaxies, and in more rarefied regions of the intergalactic space. Upper limits of $\simeq 10^{-8} - 10^{-9}$ G have been obtained for the cosmological fields at large redshift.

In this review large-scale magnetic fields in clusters of galaxies will be analyzed. In the last years the presence of cluster magnetic fields has been unambiguously proven and the importance of their role has been recently recognized. The study of cluster magnetic fields is relevant to understand the physical conditions and energetics of the intracluster medium. Cluster magnetic fields provide an additional term of pressure and may play a role in the cluster dynamics. They couple cosmic ray particles to the intracluster gas, and they are able to inhibit transport processes like heat conduction, spatial mixing of gas, and propagation of cosmic rays. They are essential for the acceleration of cosmic rays and allow cosmic ray electron population to be observed by the synchrotron radiation.

Despite many observational efforts to measure their properties, our knowledge on cluster magnetic fields is still poor. Overviews on observational and theoretical arguments can be found in the literature[1,2,3,4,5,6].

The focus of this review is primarily observational, however, we present the basic theory needed for the interpretation of the data. We analyze some of the main issues that have led to our knowledge on magnetic fields in clusters of galaxies and discuss some of their limitations. An outline of the review is as follows: In Sec. 2 we summarize some general properties of clusters of galaxies. Sec. 3 is devoted to theoretical background related to the detection of cluster magnetic fields and to the estimate of their strengths. We recall the basic theory concerning synchrotron radiation, inverse Compton radiation and Faraday rotation. These are the main

observed features which provide information on the cluster magnetic fields. The observational results of cluster magnetic fields through synchrotron radio and inverse Compton hard X-ray emissions are described in Secs. 4 and 5. In Sec. 6 we give the results obtained by analyzing rotation measures of radio galaxies located within or behind clusters of galaxies. In Sec. 7 we present cluster magnetic fields detected through the study of cold fronts. In Sec. 8 we report the evidence for a radial decline of cluster magnetic fields. In Sec. 9 we discuss how magnetic field values obtained with different approaches can be reconciled. In Sec. 10 we summarize the results of a numerical technique which can significantly improve our interpretation of the data and thus the knowledge of the strength and structure of magnetic fields. In Sec. 11 we briefly review the current knowledge on the cluster magnetic field origin and amplification.

Throughout this paper we assume the λCDM cosmology with $H_0 = 71$ km s^{-1}Mpc^{-1}, $\Omega_m = 0.3$, and $\Omega_\Lambda = 0.7$, unless stated otherwise.

2. Clusters of Galaxies

Clusters of galaxies are the largest gravitationally bound systems in the Universe. They appear at optical wavelengths as over-densities of galaxies with respect to the field average density. In addition to the galaxies, they contain an intracluster medium (ICM) of hot (T$\simeq 10^8$ K), low-density (n$_e \simeq 10^{-3}$ cm^{-3}) gas, detected through its luminous X-ray emission (L$_X \simeq 10^{43}$–10^{45} erg s^{-1}), produced by thermal bremsstrahlung radiation.

The visible galaxies and the ICM are important components of clusters, however most of the cluster mass is in dark matter. Although dark matter has not been directly observed at any wavelength and its nature remains unknown, X-ray and visible light observations provide clues to its amount and distribution in clusters.

X-ray images, starting with the *Einstein* satellite and continuing with *ROSAT* and *ASCA*, and now with *Chandra* and *XMM-Newton*, provide a powerful technique to trace the global cluster gravitational potential and to probe the dynamics, morphology and history of clusters. In the hierarchical scenario of the structures formation, clusters of galaxies are formed by the gravitational merger of smaller units e.g. groups and sub-clusters. Such mergers are spectacular events involving kinetic energies as large as $\simeq 10^{64}$ ergs. In these mergers a large portion of energy is dissipated in the ICM, generating shock, turbulence and bulk motions, and heating it. Substructure in the X-ray images as well as complex gas temperature gradients are all signatures of cluster mergers.

A significant fraction of clusters of galaxies shows the X-ray surface brightness strongly peaked at the center. This implies a high density, and cooling times of the hot ICM within the inner $\simeq 100$ kpc of much less than the Hubble time. To maintain hydrostatic equilibrium, an inward flow may be required. X-ray observations with *XMM-Newton* indicate no spectral evidence for large amounts of cooling and condensing gas in the centers of galaxy clusters believed to harbour strong cooling

flows. The cooling flow seems to be hindered by some mechanism, whose nature is still debated. Thus, there is no consensus on the actual existence of material "cooling" and "flowing". What is generally agreed upon is that cooling core clusters are more dynamically relaxed than non cooling core clusters, which often show evidence of cluster merger.

One of the most important results obtained with the *Chandra* satellite on clusters of galaxies was the discovery of sharp surface brightness discontinuities in the images of merging clusters, called "cold fronts". Initially, one might have suspected these features to be merger shocks but spectral measurements showed that these are a new kind of structure. These cold fronts are apparently contact discontinuities between the gas which was in the cool core of one of the merging sub-clusters and the surrounding intracluster gas. Cold fronts and merger shocks offer unique insights into the cluster physics, including the determination of the gas bulk velocity, its acceleration, the growth of plasma instabilities, the strength and structure of magnetic fields and the thermal conductivity.

A precise physical description of the ICM necessitates also adequate knowledge of the role of non-thermal components. The most detailed evidence for these phenomena comes from the radio observations. A number of clusters of galaxies is known to contain wide diffuse synchrotron sources (radio halos, relics and mini-halos) which have no obvious connection with the cluster galaxies, but are rather associated with the ICM. The synchrotron emission of such sources requires a population of $\approx$ GeV relativistic electrons and cluster magnetic fields on μG levels. An indirect evidence of the existence of cluster magnetic fields is also derived from studies of the Rotation Measure of radio galaxies located within or behind clusters of galaxies.

A probe of the existence of a population of relativistic electrons in the ICM is also obtained from the detection of non-thermal emission of inverse Compton origin in the hard X-ray and possibly in the extreme ultraviolet wavelengths. The combination of the observed diffuse radio and hard X-ray emissions from clusters of galaxies is used to estimate the intracluster magnetic field strengths.

3. Theoretical Background Related to Cluster Magnetic Fields

3.1. *Synchrotron radiation*

The synchrotron emission is produced by the spiraling motion of relativistic electrons in a magnetic field. It is therefore the easiest and more direct way to detect magnetic fields in astrophysical sources. The total synchrotron emission from a source provides an estimate of the strength of magnetic fields while the degree of polarization is an important indicator of the field uniformity and structure.

An electron of energy $\epsilon = \gamma m_e c^2$ (where γ is the Lorentz factor) in a magnetic field $\vec{B}$ experiences a $\vec{v} \times \vec{B}$ force that causes it to follow a helical path along the field lines, emitting radiation into a cone of half-angle $\simeq \gamma^{-1}$ about its instantaneous velocity. To the observer, the radiation is essentially a continuum with a fairly

peaked spectrum concentrated near the critical frequency

$$\nu_c = c_1(Bsin\theta)\epsilon^2. \tag{1}$$

The synchrotron power emitted by a relativistic electron is

$$-\frac{d\epsilon}{dt} = c_2(Bsin\theta)^2\epsilon^2, \tag{2}$$

where θ is the pitch angle between the electron velocity and the magnetic field direction while c_1 and c_2 depend only on fundamental physical constants

$$c_1 = \frac{3e}{4\pi m_e^3 c^5}, \qquad c_2 = \frac{2e^4}{3m_e^4 c^7}. \tag{3}$$

In practical units:

$$\begin{aligned} \nu_c[MHz] &\simeq 16.1 \times 10^6 (B_{[G]} sin\theta)(\epsilon_{[GeV]})^2 \\ &\simeq 4.2(B_{[G]} sin\theta)\gamma^2, \end{aligned} \tag{4}$$

$$\begin{aligned} -\frac{d\epsilon}{dt}\left[\frac{erg}{s}\right] &\simeq 6.0 \times 10^{-9} (B_{[G]} sin\theta)^2 (\epsilon_{[GeV]})^2 \\ &\simeq 1.6 \times 10^{-15} (B_{[G]} sin\theta)^2 \gamma^2. \end{aligned} \tag{5}$$

From Eq. 1, it is derived that electrons of $\gamma \simeq 10^4$ in magnetic fields of $B \simeq 1$ G produce synchrotron radiation in the optical domain, whereas electrons of $\gamma \simeq 10^5$ in magnetic fields of $B \simeq 10$ G radiate in the X-rays (see Fig. 1). Therefore at a given frequency, the energy (or Lorentz factor) of the emitting electrons depends directly on the magnetic field strengths. The higher is the magnetic field strength, the lower is the electron energy needed to produce emission at a given frequency. In a magnetic field of about $B \simeq 1$ μG, a synchrotron radiation detected for example at 100 MHz, is produced by relativistic electrons with $\gamma \simeq 5000$.

For an homogeneous and isotropic population of electrons with a power-law energy distribution, i.e. with the particle density between ϵ and ϵ+dϵ given by

$$N(\epsilon)d\epsilon = N_0 \epsilon^{-\delta} d\epsilon, \tag{6}$$

the total intensity spectrum, in regions which are optically thin to their own radiation, varies as:

$$S(\nu) \propto \nu^{-\alpha}, \tag{7}$$

where the spectral index $\alpha = (\delta - 1)/2$. Below the frequency where the synchrotron emitting region becomes optically thick, the total intensity spectrum can be described by:

$$S(\nu) \propto \nu^{+5/2}. \tag{8}$$

The synchrotron emission radiating from a population of relativistic electrons in a uniform magnetic field is linearly polarized. In the optically thin case, the degree of intrinsic linear polarization, for a homogeneous and isotropic distribution of relativistic electrons with a power-law spectrum as in Eq. 6, is:

$$P_{Int} = \frac{3\delta + 3}{3\delta + 7}, \tag{9}$$

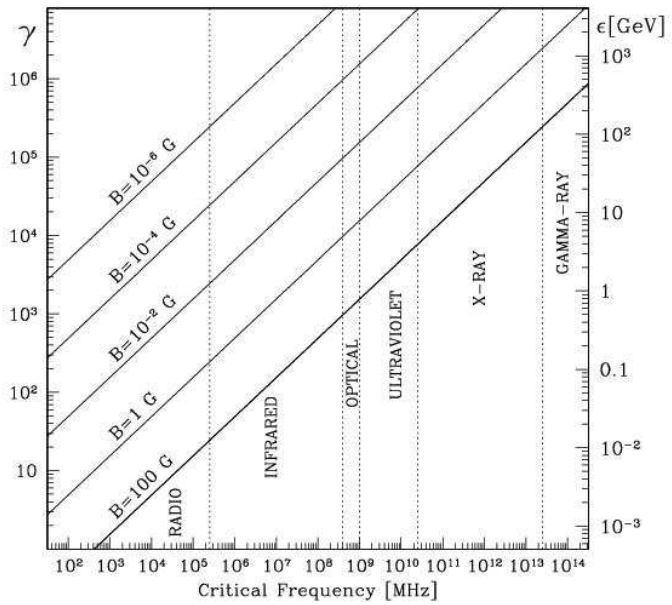


Fig. 1. Electron Lorentz factor $\gamma = \epsilon/m_e c^2$ (left-hand axis) and energy (right-hand axis) versus synchrotron critical frequency for magnetic field strengths in the range $10^{-6} - 100$ G (θ=90°).

with the electric (polarization) vector perpendicular to the projection of the magnetic field onto the plane of the sky. For typical values of the particle spectral index, the intrinsic polarization degree is $\sim 75 - 80\%$. In the optically thick case:

$$P_{Int} = \frac{3}{6\delta + 13} \tag{10}$$

and the electric vector is parallel to the projected magnetic field.

In practice, the polarization degree detected in radio sources is much lower than expected by the above equations. A reduction in polarization could be due to a complex magnetic field structure whose orientation varies either with depth in the source or over the angular size of the beam. For instance, if one describes the magnetic field inside an optically thin source as the superposition of two components, one uniform B_u, the other isotropic and random B_r, the observed degree of polarization can be approximated by[7]:

$$P_{Obs} = P_{Int} \frac{B_u^2}{B_u^2 + B_r^2}. \tag{11}$$

A rigorous treatment of how the degree of polarization is affected by the magnetic field configuration is presented by Sokoloff et al.[8,9]

3.2. *Equipartition magnetic fields derived from the synchrotron emission*

From the synchrotron emissivity it is not possible to derive unambiguously the magnetic field value. The usual way to estimate the magnetic field strength in a radio source is to minimize its total energy content U_{tot}[10]. The total energy of a synchrotron source is due to the energy in relativistic particles (U_{el} in electrons and U_{pr} in protons) plus the energy in magnetic fields (U_B):

$$U_{tot} = U_{el} + U_{pr} + U_B. \tag{12}$$

The magnetic field energy contained in the source volume V is given by

$$U_B = \frac{B^2}{8\pi}\Phi V, \tag{13}$$

where Φ is the fraction of the source volume occupied by the magnetic field (filling factor). The electron total energy in the range $\epsilon_1 - \epsilon_2$:

$$U_{el} = V \times \int_{\epsilon_1}^{\epsilon_2} N(\epsilon)\epsilon \, d\epsilon = V N_0 \int_{\epsilon_1}^{\epsilon_2} \epsilon^{-\delta+1} \, d\epsilon \tag{14}$$

can be expressed as a function of the synchrotron luminosity L_{syn}:

$$L_{syn} = V \times \int_{\epsilon_1}^{\epsilon_2} \left(-\frac{d\epsilon}{dt}\right) N(\epsilon) \, d\epsilon = c_2 (B sin\theta)^2 V N_0 \int_{\epsilon_1}^{\epsilon_2} \epsilon^{-\delta+2} \, d\epsilon \tag{15}$$

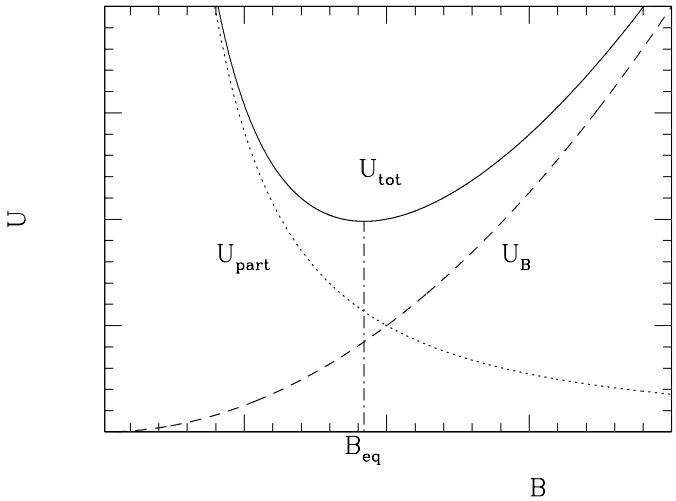


Fig. 2. Energy content in a radio source (in arbitrary units): the energy in magnetic fields is $U_B \propto \mathrm{B}^2$, the energy in relativistic particles is $U_{part} = U_{el} + U_{pr} \propto \mathrm{B}^{-3/2}$. The total energy content U_{tot} is minimum when the contributions of magnetic fields and relativistic particles are approximately equal (equipartition condition). The corresponding magnetic field is commonly referred to as equipartition value B_{eq}.

by eliminating VN_0 and by writing ϵ_1 and ϵ_2 in terms of ν_1 and ν_2 (Eq. 1):

$$U_{el} = c_2^{-1} c_1^{1/2} \tilde{C}(\alpha, \nu_1, \nu_2) L_{syn} B^{-3/2} = c_{12}(\alpha, \nu_1, \nu_2) L_{syn} B^{-3/2}, \tag{16}$$

where $sin\theta$ has been taken equal to 1 and

$$\tilde{C}(\alpha, \nu_1, \nu_2) = \left(\frac{2\alpha - 2}{2\alpha - 1}\right) \frac{\nu_1^{(1-2\alpha)/2} - \nu_2^{(1-2\alpha)/2}}{\nu_1^{(1-\alpha)} - \nu_2^{(1-\alpha)}}. \tag{17}$$

The energy contained in the heavy particles, U_{pr}, can be related to U_{el} assuming:

$$U_{pr} = kU_{el}. \tag{18}$$

Finally the total energy is obtained as a function of the magnetic field:

$$U_{tot} = (1 + k) c_{12} L_{syn} B^{-3/2} + \frac{B^2}{8\pi} \Phi V. \tag{19}$$

In order to obtain an estimate for the magnetic fields, it is necessary to make some assumptions about how the energy is distributed between the fields and particles. A convenient estimate for the total energy is represented by its minimum value (see Fig. 2). The condition of minimum energy is obtained when the contributions of the magnetic field and the relativistic particles are approximately equal:

$$U_B = \frac{3}{4}(1 + k) U_{el}. \tag{20}$$

For this reason the minimum energy is known as equipartition value:

$$U_{tot}(min) = \frac{7}{4}(1 + k) U_{el} = \frac{7}{3} U_B. \tag{21}$$

The magnetic field for which the total energy content is minimum is:

$$B_{eq} = (6\pi(1 + k) c_{12} L_{syn} \Phi^{-1} V^{-1})^{2/7}. \tag{22}$$

The total minimum energy is:

$$U_{tot}(min) = c_{13} \left(\frac{3}{4\pi}\right)^{3/7} (1 + k)^{4/7} \Phi^{3/7} V^{3/7} L_{syn}^{4/7}, \tag{23}$$

and the total minimum energy density is:

$$u_{min} = \frac{U_{tot}(min)}{V\Phi} = c_{13} \left(\frac{3}{4\pi}\right)^{3/7} (1 + k)^{4/7} \Phi^{-4/7} V^{-4/7} L_{syn}^{4/7}, \tag{24}$$

where $c_{13} = 0.921 c_{12}^{4/7}$. The constants c_{12} and c_{13}, depending on the spectral index and on the frequency range, are tabulated[10] for cgs units.

By including the K-correction, assuming $\Phi = 1$, and expressing the parameters in commonly used units, we can write the minimum energy density of a radio source in terms of observed quantities:

Table 1. Equipartition parametrization

α	$\xi(\alpha$, 10 MHz, 10 GHz)	$\xi(\alpha$, 10 MHz, 100 GHz)
0.0	1.43×10^{-11}	2.79×10^{-11}
0.1	9.40×10^{-12}	1.63×10^{-11}
0.2	6.29×10^{-12}	9.72×10^{-12}
0.3	4.29×10^{-12}	5.97×10^{-12}
0.4	2.99×10^{-12}	3.79×10^{-12}
0.5*	2.13×10^{-12}	2.50×10^{-12}
0.6	1.55×10^{-12}	1.72×10^{-12}
0.7	1.15×10^{-12}	1.23×10^{-12}
0.8	8.75×10^{-13}	9.10×10^{-13}
0.9	6.77×10^{-13}	6.92×10^{-13}
1.0*	5.32×10^{-13}	5.39×10^{-13}
1.1	4.24×10^{-13}	4.27×10^{-13}
1.2	3.42×10^{-13}	3.43×10^{-13}
1.3	2.79×10^{-13}	2.79×10^{-13}
1.4	2.29×10^{-13}	2.29×10^{-13}
1.5	1.89×10^{-13}	1.89×10^{-13}
1.6	1.57×10^{-13}	1.57×10^{-13}
1.7	1.31×10^{-13}	1.31×10^{-13}
1.8	1.10×10^{-13}	1.10×10^{-13}
1.9	9.21×10^{-14}	9.21×10^{-14}
2.0	7.76×10^{-14}	7.76×10^{-14}

*for these values of α the constant defined in Eq. 17 diverges, thus the corresponding parameters have been computed by solving directly the integrals in Eqs. 14 and 15.

$$u_{min}\left[\frac{erg}{cm^3}\right] = \xi(\alpha,\nu_1,\nu_2)(1+k)^{4/7}(\nu_{0[MHz]})^{4\alpha/7}(1+z)^{(12+4\alpha)/7}\times \qquad (25)$$

$$\times\,(I_{0[\frac{mJy}{arcsec^2}]})^{4/7}(d_{[kpc]})^{-4/7},$$

where z is the source redshift, I_0 is the source brightness at the frequency ν_0, d is the source depth, and the constant $\xi(\alpha,\nu_1,\nu_2)$ is tabulated in Table 1 for the frequency ranges: 10 MHz−10 GHz and 10 MHz−100 GHz. I_0 can be measured directly by the contour levels of a radio image (for significantly extended sources), or can be obtained by dividing the source total flux by the source solid angle.

The equipartition magnetic field is then obtained as:

$$B_{eq} = \left(\frac{24\pi}{7}u_{min}\right)^{1/2}. \qquad (26)$$

One must be aware of the uncertainties inherent to this determination of the magnetic field strength. The value of k, ratio of the energy in relativistic protons to that in electrons, depends on the mechanism of generation of relativistic electrons, which is so far poorly known. Uncertainties are also related to the volume filling factor Φ. Values usually assumed in literature for clusters are $k = 1$ (or $k = 0$) and $\Phi = 1$. Another parameter difficult to infer is the extent of the source along the line of sight d.

In the standard approach presented above, the computation of equipartition parameters is based on the integration of the synchrotron radio luminosity between the two fixed frequencies ν_1 and ν_2 (Eq. 16 and followings). The electron energies corresponding to these frequencies depend on the magnetic field value (see Eq. 1), thus the integration limits are variable in terms of the energy of the radiating electrons. The lower limit is particularly relevant, owing to the power-law shape of the electron energy distribution and to the fact that electrons of very low energy are expected to be present. If a low-energy cutoff in the particle energy distribution is imposed, rather than a low-frequency cut-off in the emitted synchrotron spectrum, the exponent 2/7 in Eq. 22 should be replaced by $1/(3+\alpha)$, as pointed out by Beck & Krause[11]. The equipartition quantities obtained following this approach are presented by Brunetti et al.[12]. Indicating the electron energy by its Lorentz factor γ, assuming that $\gamma_{min} << \gamma_{max}$, the new expression for the equipartition magnetic field B'_{eq} in Gauss is (for $\alpha > 0.5$):

$$B'_{eq} \sim 1.1 \; \gamma_{min}^{\frac{1-2\alpha}{3+\alpha}} \; B_{eq}^{\frac{7}{2(3+\alpha)}}, \tag{27}$$

where B_{eq} is the value of the equipartition magnetic field obtained with the standard formulae by integrating the radio spectrum between 10 MHz and 100 GHz. If the equipartition magnetic field obtained with the standard formulae is $\sim \mu$G, the magnetic field derived considering electrons of $\gamma_{min} \sim 100$ is 2 to 5 times larger, using α in the range $0.75 - 1$.

3.3. *Inverse Compton radiation*

Relativistic electrons in a radiation field can scatter and transfer energy to photons through the inverse-Compton (IC) effect. This situation where the wave gains energy from the electron is the inverse of the usual Compton scattering. The frequency of the scattered wave ν_{out} is related to that of the incident wave ν_{in} as:

$$\nu_{out} = \frac{4}{3}\gamma^2 \nu_{in}. \tag{28}$$

In astrophysical applications, the IC plays a very important role since the relativistic electron population responsible for synchrotron emission scatters the ubiquitous 3K microwave background photons. The Planck function at T = 2.73 K peaks near a frequency of $\nu \sim 1.6 \times 10^{11}$ Hz, therefore from Eq. 28 the relativistic electrons of energy $\gamma = 1000 - 5000$ will be responsible for IC emission in the X-ray domain, respectively at $\sim 2 \times 10^{17} - 5.3 \times 10^{18}$ Hz, corresponding to $\sim 0.9 - 22$ keV. Microwave background photons are then turned into X-ray or gamma photons.

Given that synchrotron and IC emission originate from the same, assumed power-law, relativistic electron population (Eq. 6), they share the same spectral index α. The spectral index relates to the index of the power-law electron energy density distribution as $\delta = 2\alpha + 1$, and to the photon index of the IC emission as $\Gamma_X = \alpha + 1$.

3.4. *Magnetic fields derived from IC emission*

When the synchrotron radio and IC X-ray emission are produced by the same population of relativistic electrons (see Secs. 3.1 and 3.3), the total synchrotron and IC powers are related. The IC emissivity is proportional to the energy density in the photon field, u_{ph}, which for the cosmological blackbody radiation is $\sim 5 \times 10^{-13}$ (1+z)^4 erg cm^{-3}, whereas the synchrotron emissivity is proportional to the energy density in the magnetic field, $u_B = B^2/8\pi$. This leads to a simple proportionality between synchrotron and IC luminosities:

$$\frac{L_{syn}}{L_{IC}} \propto \frac{u_B}{u_{ph}}. \tag{29}$$

Combining the standard formulae of the synchrotron and Compton emission mechanisms, the radio and HXR detections directly yield some of the basic properties of the magnetic field. Following Blumenthal and Gould[13], the synchrotron flux at the radio frequency ν_r and the IC X-ray flux at frequency ν_x are (all parameters in cgs units):

$$S_{syn(\nu_r)} = 1.7 \times 10^{-21} \frac{VN_0}{4\pi D^2} a(\delta) B^{1+\alpha} \left(\frac{4.3 \times 10^6}{\nu_r} \right)^{\alpha}, \tag{30}$$

$$S_{IC(\nu_x)} = 4.2 \times 10^{-40} \frac{VN_0}{4\pi D^2} b(\delta) T^{3+\alpha} (1+z)^{3+\alpha} \left(\frac{2.1 \times 10^{10}}{\nu_x} \right)^{\alpha}, \tag{31}$$

where the functions a(δ) and b(δ) are tabulated in Table 2, V is the emission volume, and D the source distance. From the ratio between the X-ray and radio fluxes, one derives an estimate of the total magnetic field, averaged over the emitting volume.

To obtain a formula for practical use, we first relate the monochromatic X-ray flux $S_{IC(\nu_x)}$ to the flux $S_{IC(E_1-E_2)}$ integrated over the energy interval $E_1 - E_2$, as this is the parameter usually measured from observations:

$$S_{IC(E_1-E_2)} \propto S_{IC(\nu_x)} \frac{E_2^{1-\alpha} - E_1^{1-\alpha}}{1-\alpha} (\nu_x)^{\alpha}. \tag{32}$$

We also substitute the radiation temperature T = 2.7 K at z = 0, and we compute the constants for commonly used units. We obtain the magnetic field as:

$$(B[\mu G])^{1+\alpha} = h(\alpha) \frac{S_{syn(\nu_r)}[Jy]}{S_{IC(E_1-E_2)}[ergs^{-1}cm^{-2}]} (1+z)^{3+\alpha} (0.0545 \nu_r[MHz])^{\alpha} \times \tag{33}$$

$$\times (E_2[keV]^{1-\alpha} - E_1[keV]^{1-\alpha}),$$

where the function h(α) is tabulated in Table 2. For $\alpha = 1$, the above formula becomes

$$(B[\mu G])^2 = 10^{-16} \frac{S_{syn(\nu_r)[Jy]}}{S_{IC(E_1-E_2)}[ergs^{-1}cm^{-2}]} (1+z)^4 \frac{\nu_r}{[MHz]} \left(ln \frac{E_2[keV]}{E_1[keV]} \right). \tag{34}$$

The difficulties related to this method are essentially due to the limitations of present X-ray observations in the hard X-ray domain and to the problem of distinguishing

Table 2. Inverse Compton parametrization

α	δ	a(δ)	b(δ)	h(α)
0.0	1	0.283	3.20	1.32×10^{-16}
0.1	1.2	0.209	3.42	2.13×10^{-16}
0.2	1.4	0.164	3.73	3.31×10^{-16}
0.3	1.6	0.136	4.12	5.06×10^{-16}
0.4	1.8	0.117	4.62	7.71×10^{-16}
0.5	2.0	0.103	5.25	1.19×10^{-15}
0.6	2.2	0.093	6.03	1.89×10^{-15}
0.7	2.4	0.086	7.00	3.17×10^{-15}
0.8	2.6	0.081	8.20	5.95×10^{-15}
0.9	2.8	0.077	9.69	1.48×10^{-14}
1.0	3.0	0.074	11.54	see Eq. 34
1.1	3.2	0.072	13.85	-2.24×10^{-14}
1.2	3.4	0.071	16.74	-1.37×10^{-14}
1.3	3.6	0.071	20.35	-1.12×10^{-14}
1.4	3.8	0.072	24.89	-1.02×10^{-14}
1.5	4.0	0.073	30.62	-9.88×10^{-15}
1.6	4.2	0.075	37.87	-9.96×10^{-15}
1.7	4.4	0.076	47.07	-1.03×10^{-14}
1.8	4.6	0.079	58.78	-1.09×10^{-14}
1.9	4.8	0.083	73.74	-1.16×10^{-14}
2.0	5.0	0.087	92.90	-1.25×10^{-14}

between the non-thermal and the thermal X-ray emission. When the IC X-ray emission is not detected from a radio emitting region, only lower limits to the magnetic fields can be derived.

3.5. *Faraday Rotation effect*

The Faraday rotation effect appears during the propagation of electromagnetic waves in a magnetized plasma. A linearly polarized wave can be decomposed into opposite-handed circularly polarized components. The right-handed and left-handed circularly polarized waves propagate with different phase velocities within the magneto-ionic material. This effectively rotates the plane of polarization of the electromagnetic wave.

According to the dispersion relation, for a wave of angular frequency ω ($\omega = 2\pi\nu$), the refractive index of a magnetized dielectric medium can take two possible values:

$$n_{L,R} = \left(1 - \frac{\omega_p^2}{\omega^2 \pm \omega\Omega_e}\right)^{1/2}, \tag{35}$$

where $\omega_p = (\frac{4\pi n_e e^2}{m_e})^{1/2}$ is the plasma frequency, and $\Omega_e = \frac{eB}{m_e c}$ is the cyclotron frequency.

In the context of the study of cluster magnetic fields we are interested in the Faraday rotation of radio sources in the background of the cluster or in the cluster

itself. The radio frequencies dominate the values of ω_p and Ω_e obtained for typical magnetic fields ($B \simeq 1\mu$G) and gas densities ($n_e \simeq 10^{-3}$ cm^{-3}) in the ICM. In the limit $\omega >> \Omega_e$, Eq. 35 can be approximated as:

$$n_{L,R} \approx 1 - \frac{1}{2}\frac{\omega_p^2}{(\omega^2 \pm \omega\Omega_e)}, \tag{36}$$

thus the difference in time of the two opposite handed waves to travel a path length dl results:

$$\Delta t \approx \frac{\omega_p^2 \Omega_e dl}{c\omega^3} = \frac{4\pi e^3}{\omega^3 m_e^2 c^2} n_e B dl \tag{37}$$

and the phase difference between the two signals is $\Delta\phi = \omega\Delta t$. Therefore, traveling along the cluster path length L, the intrinsic polarization angle Ψ_{Int} will be rotated by an angle $\Delta\Psi{=}\frac{1}{2}\Delta\phi$, resulting:

$$\Psi_{Obs}(\lambda) = \Psi_{Int} + \Delta\Psi = \Psi_{Int} + \frac{e^3\lambda^2}{2\pi m_e^2 c^4}\int_0^L n_e(l) B_\parallel(l) dl, \tag{38}$$

where $B_\parallel$ is the component of the magnetic field along the line of sight. Ψ_{Obs} is usually written in terms of the rotation measure, RM:

$$\Psi_{Obs}(\lambda) = \Psi_{Int} + \lambda^2 RM, \tag{39}$$

where:

$$RM = \frac{e^3}{2\pi m_e^2 c^4}\int_0^L n_e(l) B_\parallel(l) dl. \tag{40}$$

In practical units:

$$RM\left[\frac{rad}{m^2}\right] = 812\int_0^L n_e[cm^{-3}] B_\parallel[\mu G] dl[kpc]. \tag{41}$$

By convention, RM is positive (negative) for a magnetic field directed toward (away from) the observer.

The position angle of the polarization plane Ψ_{Obs} is an observable quantity, therefore, the RM of radio sources can be derived by a linear fit to Eq. 39. In general, the position angle must be measured at three or more wavelengths in order to determine RM accurately and remove the $\Psi_{Obs} = \Psi_{Obs} \pm n\pi$ ambiguity.

3.5.1. *Depolarization due to Faraday rotation*

The term depolarization indicates a decrease of the polarization percentage, either at a given frequency, or when comparing two different frequencies. In a radio source the observed degree of polarization intensity, $P_{Obs}(\lambda)$, can be significantly lower with respect to the intrinsic value, P_{Int}, if differential Faraday rotation occurs. The

Faraday rotation can induce a depolarization of the observed radiation in different circumstances.

External depolarization is induced by the limitations of the instrumental capabilities. Beamwidth depolarization is due to the presence of fluctuations in the foreground screen within the observing beam: unresolved density or magnetic field inhomogeneities of the media through which the radiation propagates induce unresolved spatial variation in the Faraday rotation measure and hence beam depolarization. In addition, bandwidth depolarization occurs when a significant rotation of the polarization angle of the radiation is produced across the observing bandwidth.

Internal depolarization is due to the spatial extent of the source itself and occurs even if the intervening media are completely homogeneous. Along the line of sight, the emission from individual electrons within a source arises from different depths and suffers different Faraday rotation angles due to the different path length. For the total radiation emitted by the source, this results in a reduction of the observed degree of polarization. In the case that the Faraday effect originates entirely within the source, when the source can be represented by an homogeneous optically thin slab, the degree of polarization varies as[7]:

$$P_{Obs}(\lambda) = P_{Int} \frac{sin(RM'\lambda^2)}{RM'\lambda^2}, \tag{42}$$

where RM' is the internal Rotation Measure through the depolarizing source. If a value of the Rotation Measure RM_{Obs} is derived observationally from the rotation of the polarization angle, then RM' in the above equation is $= 2\ RM_{Obs}$[8,9]. Indeed the observed rotation is the average of the full rotation occurring across the source, thus it is 1/2 of the total back-to-front rotation.

To distinguish between the external and internal depolarization, very high resolution and sensitive polarization data at multiple frequencies are needed. The key difference between them is that internal depolarization should be correlated with the Faraday rotation measure, therefore regions with small RM should exhibit very little depolarization. Instead, the external beam depolarization, due to gradients in the RM, should not be correlated with the amount of the RM but with the amount of the RM gradient.

3.5.2. *Interpretation of the cluster RM data*

RM data of radio sources in the background of clusters or in the clusters themselves, together with a model for the intracluster gas density distribution, can provide important information on the cluster magnetic field responsible for the Faraday effect. The Faraday effect of an external screen containing a gas with a constant density and a uniform magnetic field produces no depolarization and a rotation of the polarization angle proportional to $\lambda^2\langle \mathrm{RM} \rangle$, with:

$$\langle RM \rangle = 812 B_{\parallel} n_e L. \tag{43}$$

The existence of small-scale magnetic field structures produce both rotation of the polarization angle and depolarization.

The effect of Faraday rotation from a tangled magnetic field has been analyzed by several authors[8,9,14,15,16,17], in the simplest approximation that the magnetic field is tangled on a single scale Λ_c. In this ideal case, the screen is made of cells of uniform size, electron density and magnetic field strength, but with a field orientation at random angles in each cell. The observed RM along any given line of sight is then generated by a random walk process involving a large number of cells of size Λ_c. The distribution of the RM is Gaussian with $\langle \mathrm{RM} \rangle = 0$, and variance given by:

$$\sigma^2_{RM} = \langle RM^2 \rangle = 812^2 \Lambda_c \int (n_e B_\parallel)^2 dl \ . \tag{44}$$

In this formulation, by considering a density distribution which follows a β-profile[18]:

$$n_e(r) = n_0 (1 + r^2/r_c^2)^{-3\beta/2}, \tag{45}$$

the following relation for the RM dispersion as a function of the projected distance from the cluster center, $r_\perp$, is obtained by integrating Eq. 44:

$$\sigma_{RM}(r_\perp) = \frac{K B n_0 r_c^{1/2} \Lambda_c^{1/2}}{(1 + r_\perp^2/r_c^2)^{(6\beta-1)/4}} \sqrt{\frac{\Gamma(3\beta - 0.5)}{\Gamma(3\beta)}}, \tag{46}$$

where Γ is the Gamma function. The constant K depends on the integration path over the gas density distribution: $K = 624$, if the source lies completely beyond the cluster, and $K = 441$ if the source is halfway through the cluster.

Therefore, since the density profile of the ICM can be obtained by X-ray observations, the cluster magnetic field strength can be estimated by measuring σ_{RM} from spatially resolved RM images of radio sources if Λ_c is inferred or is known.

4. Diffuse Radio Emission in Clusters of Galaxies

The presence of magnetic fields in clusters is directly demonstrated by the existence of large-scale diffuse synchrotron sources, that have no apparent connection to any individual cluster galaxy and are therefore associated with the ICM. These radio sources have been classified as radio halos, relics and mini-halos depending on their morphology and location. Radio halos, relics and mini-halos are not a common phenomenon in clusters and until recently they were known to exist in only a handful of clusters of galaxies[19]. This was a consequence of the fact that they show low surface brightness, large size and steep spectrum, thus they are difficult to reveal. Extended, low-brightness structures are most easily detected with filled-aperture telescopes, but the low resolving power of single-dish radio telescopes increases problems with confusion and can create an apparent wide source from a blend of weak discrete radio sources. Observations made with interferometers have the angular resolution necessary to separate the individual radio galaxies, but generally lack information from short spacing, thus hindering the detection of extended low-brightness structures.

The number of clusters with known diffuse sources has increased in the last few years to around 50, thanks to the improved sensitivity of radio telescopes and the existence of deep surveys. New halo and relic candidates were found from searches in the NRAO VLA Sky Survey (NVSS[20]) by Giovannini et al.[21], in the Westerbork Northern Sky Survey (WENSS[22]) by Kempner and Sarazin[23], in the Sidney University Molonglo Sky Survey (SUMSS[24]) by Hunstead et al.[25] and in the survey of the Sharpley Concentration by Venturi et al.[26].

The presence of these large regions of diffuse synchrotron emission reveals a large-scale distribution of $\approx$ GeV relativistic electrons radiating in $\sim \mu$G magnetic fields, in the ICM.

4.1. *Radio halos*

Cluster radio halos are the most spectacular expression of clusters non-thermal emission. They permeate the cluster centers with size of more than a Mpc, showing low surface brightnesses ($\simeq 10^{-6}$Jy arcsec^{-2} at 21 cm) and steep spectra ($\alpha \gtrsim 1$). A typical example is Coma C, the halo source in the Coma cluster, which was first shown to be diffuse by Willson[27] and mapped later at various radio wavelengths by several authors[28,29,30,31,32,33,34,35,36,37]. In Fig. 3 we show a radio image at 90 cm of the Coma cluster[34], obtained with the Westerbork Synthesis Radio Telescope (WSRT). The integrated spectrum of Coma C is $\alpha \simeq 1.3$, with a steepening at high frequencies[37]. The spectral index distribution shows a radial decrease from $\alpha \sim 0.8$ at the cluster center, to $\alpha \sim 1.8$ at about $15'$ from the center[34].

Studies of several radio halos and of their hosting clusters have been recently performed, thus improving the knowledge of the characteristics and physical properties of this class of radio sources. Radio halos have been studied in X-ray luminous clusters such as A2163[38] and 1E0657-57[39], and in distant clusters, such as A2744[40] (z = 0.308), and CL0016+16[41] (z = 0.5545). The latter is the most distant cluster with a radio halo known so far. Halos of small size, i.e. $\sim$ 500-600 kpc have also been detected in some cases (e.g. in A2218[41] and in A3562[42]).

No polarized flux has been detected so far in radio halos. In the Coma cluster, the upper limit to the fractional polarization of Coma C is of $\sim 10\%$ at 1.4 GHz[34]. Upper limits of $\sim 6.5\%$ and of $\sim 4\%$ have been obtained for the two powerful radio halos in A2219[43] and A2163[38], respectively. Also, no significant polarization is reported for 1E0657-57[39]. The interpretation of these low polarization levels is that the thermal gas has become mixed with the relativistic plasma, thus internal depolarization occurs within the radio emitting plasma. In addition, the magnetic field may be disordered on scales smaller than the observing beam, thus producing significant beam depolarization.

Due to their low surface brightness, radio halos have been studied so far with low spatial resolution. This prevents a detailed investigation of the small-scale magnetic field geometry and intensity. Using minimum energy assumptions (see Sec. 3.2), it is possible to estimate an equipartition magnetic field strength averaged over the

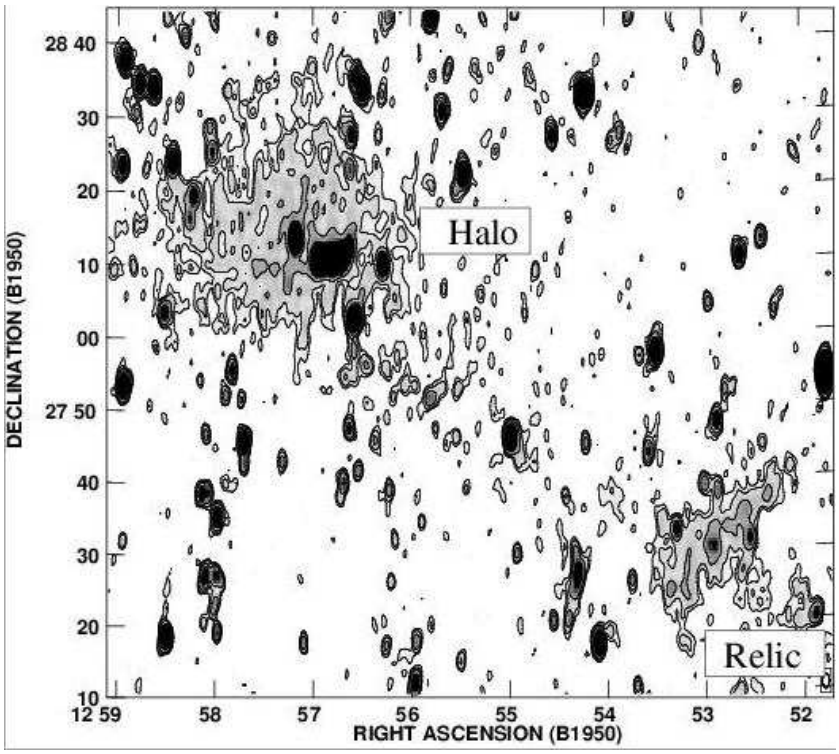


Fig. 3. WSRT radio image[34] of the Coma cluster at 90 cm with a resolution (FWHM) of $55'' \times 125''$(RA $\times$ DEC). The cluster center is approximately located at the position $\mathrm{RA}_{1950} = 12^h\ 57^m\ 24^s$, $\mathrm{DEC}_{1950} = 28°15'00''$. The radio halo Coma C is at the cluster center, the radio relic 1253+275 is at the cluster periphery. The gray-scale range display total intensity emission from 2 to 30 mJy/beam whereas contour levels are at 3, 5, 10, 30, 50 mJy/beam. The Coma cluster is at a redshift of 0.023, such that $1''$ is 0.46 kpc.

entire halo volume, i.e. on scales as large as ~ 1 Mpc. The derived minimum energy densities in halos are of the order of $10^{-14} - 10^{-13}$ erg cm^{-3}, i.e. much lower than the energy density in the thermal gas. These calculations typically assume equal energy in relativistic protons and electrons (k = 1), a volume filling factor $\Phi = 1$, a low frequency cut-off of 10 MHz, and a high frequency cut-off of 10 GHz. The corresponding equipartition magnetic field strengths range from $\simeq 0.1$ to 1 μG. In the Coma cluster, a minimum energy density of 1.9×10^{-14} erg cm^{-3} is derived from the radio data in Coma C. The corresponding[34] equipartition magnetic field is 0.45 μG. In the equipartition approximation, a homogeneous cluster magnetic field is assumed, but this is probably a too simple picture. Important clues about a radial decrease of the magnetic field strength in clusters of galaxies are given in Sec. 8.

Several models for the origin of the relativistic radiating electrons in the ICM have been proposed (see, e.g., recent reviews[44,45,46,47] and references therein). These can be basically divided in two different scenarios:

• *Primary electron* models[48,49] in which relativistic electrons are injected in the ICM from AGN activity (quasar, radio galaxies, etc.) and/or from star formation in galaxies (supernovae, galactic winds, etc.). The radiative lifetime of the relativistic electrons is relatively short ($\sim 10^{7-8}$ yrs). Therefore models involving a primary origin of the relativistic electrons require continuous injection processes and/or reacceleration processes in order to explain the presence of diffuse non-thermal emission out to Mpc scales. Electrons are likely reaccelerated in the gas turbulence[31,50,51,52] or in shocks[53,54,55], although the efficiency of the latter process is debated[56,57].

• *Secondary electron* models[58,59,60] in which cosmic ray electrons result as secondary products of hadronic collisions between relativistic protons and ICM thermal protons. The relativistic protons in the ICM have lifetimes of the order of the Hubble time. Thus they are able to travel a large distance from their source before they release their energy. In this way, electrons are produced through the whole cluster volume and do not need to be reaccelerated. The production of relativistic electrons by secondary models predict large gamma-ray fluxes from neutral pion decay which could be tested by future gamma-ray missions.

On the observational side, it is possible to draw some of the general characteristics of radio halos and derive correlations with other cluster properties:

i) Halos are typically found in clusters with significant substructure and deviation from spherical symmetry in the X-ray morphology[61,62]. This is confirmed by the high resolution X-ray data obtained with *Chandra* and *XMM*[63,64,65,66,67,68,69]. In addition to the distorted X-ray morphology, all the clusters with halos exhibit strong gas temperature gradients. Some clusters show a spatial correlation between the radio halo brightness and the hot gas regions, although this is not a general feature[68].
ii) In a number of well-resolved clusters, a point-to-point spatial correlation is observed between the radio brightness of the halo and the X-ray brightness as detected by *ROSAT*[70]. This correlation is visible e.g. in A2744 also in the *Chandra* high resolution data[67].
iii) Halos are present in rich clusters, characterized by high X-ray luminosities and temperatures[71]. The percentage of clusters with halos in a complete X-ray flux-limited sample (that includes systems with $L_X > 5 \times 10^{44} h_{50}^{-2}$ erg s^{-1} in the $0.1-2.4$ keV band) is $\simeq 5\%$. The halo fraction increases with the X-ray luminosity, to $\simeq 33\%$ for clusters with $L_X > 10^{45} h_{50}^{-2}$ erg s^{-1}.
iv) The radio power of a halo strongly correlates with the cluster luminosity[39,43,72] the gas temperature[39,73], and the total mass[40].

Therefore the available data suggest that radio halos seem to be strictly related to the X-ray properties of the host clusters and to the presence of cluster merger processes, which can provide the energy for the electron reacceleration and mag-

netic field amplification on large scales. From energetic grounds, mergers can indeed supply enough kinetic energy for the maintenance of a radio halo, as first suggested by Harris et al.[74].

The observed link between radio halos and cluster mergers is in favor of primary electron models. These are also supported by the high frequency steepening of the integrated radio spectra (e.g. in Coma C[37]) and by the radial steepening of the two-frequency spectra in Coma C[34], A665[75] and A2163[75]. These spectral behaviors can be easily reproduced by models invoking reacceleration of particles. On the contrary, they are difficult to explain by models considering secondary electron populations.

4.2. *Relics*

Radio relics are a class of diffuse sources typically located near the periphery of the cluster. Unlike the halos, they show an elongated or irregular shape and are strongly polarized. The prototype of this class is 1253+275, in the Coma cluster (see Fig. 3), first classified by Ballarati et al.[76]. The polarization of 1253+275 at 20 cm is $25 - 30\%$[37,77]. The magnetic field is oriented along the source major axis and the magnetic field strength derived from minimum energy arguments of the synchrotron emitting plasma is 0.55 μG.

A complex radio emission is detected in A2256[78,79], which contains several head-tail radio galaxies, two large regions of diffuse radio relic emission and a central radio halo. The relics are highly polarized[80], with the linear fractional polarization at 20 cm above 30% for the majority of the region, reaching values up to 50%. The intrinsic magnetic field direction reveals that there is a large-scale order to the fields, and it appears to trace the bright filaments in the relics.

In addition to Coma and A2256, other clusters present both a central halo and a peripheral relic, e.g. A2255[81,82], A1300[83], A2744[40] and A754[43,84]. A spectacular example of two almost symmetric relics in the same cluster is found in A3667[85,86].

A puzzling relic source is 0917+75[41,87], located at 5 to 8 Mpc from the centers of the closest clusters (A762, A786, A787), thus not unambiguously associated with any of them. It has a high fractional polarization (up to 48% at 20 cm and 60% at 6 cm for the brightest parts of the source) and the magnetic field direction appears to be coherent over scales of at least several hundreds kpc.

The equipartition magnetic fields in the relics, computed with standard assumptions (k = 1, $\Phi = 1$, $\nu_1 = 10$ MHz, $\nu_2 = 10$ GHz), are in the range $0.5 - 2\ \mu$G[40,77,88]. We note, however, that they refer to regions where the cluster magnetic fields are expected to be compressed (see below), thus they are not indicative of the overall magnetic field intensity in the peripheral cluster regions.

In recent years, there has been increasing evidence that the relics are related to ongoing merger events. It has been suggested that relics result from first order Fermi acceleration of relativistic particles in shocks produced during cluster merger events[55,88,89,90]. Enßlin and Brüggen[91] presented 3-D magneto hydrodynamic (MHD) simulations of electrons reaccelerated by adiabatic compression[92] of

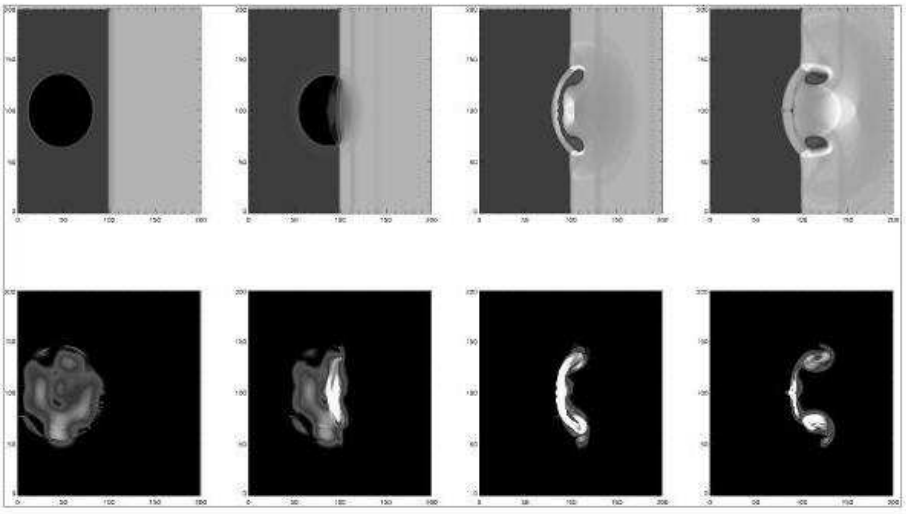


Fig. 4. 3-D MHD simulations[91] of electrons reaccelerated by compression of existing cocoons of radio plasma that traverses a shock wave. In figure is shown the passage of a radio cocoon through a shock wave and the consequent evolution of the gas density (top) and magnetic field energy density (bottom).

existing cocoons of radio plasma that traverses a shock wave. The passage of a radio cocoon through a shock wave and the consequent evolution of the gas density and magnetic field energy density can be seen in Fig. 4. This model is consistent with the relic elongated structure almost perpendicular to the merger axis. Moreover, the derived maps obtained in the simulations reproduce very well the filamentary structure seen in relic sources at high resolution[93].

The observed high polarization fraction of the relics should result from the compression of the wave, which aligns unordered magnetic fields with the shock front. Due to the low gas density, a low Faraday effect is expected at the cluster periphery, even in the presence of a tangled magnetic field.

4.3. *Mini-halos*

There are a few clusters where the relativistic electrons can be traced out quite far from the central galaxy, forming what is called mini-halo. Mini-halos are diffuse steep-spectrum radio sources, extended on a moderate scale (up to $\simeq$ 500 kpc), surrounding a dominant radio galaxy at the cluster center. Unlike radio halos and relics, mini-halos are not tied to on-going merger events in clusters, as they are typically found at the center of cooling core, i.e relaxed, clusters. The prototype example of a mini-halo is at the center of the Perseus cluster. The size is $\sim$ 450 kpc, with no significant polarization[94,95]. The strong polarized emission, detected through the entire cluster at 92 cm, at a Faraday depth ($\sim 25 - 90$ rad m^{-2}) higher than the galactic contribution seems not to be related to the mini-halo[96].

Other examples of mini-halos are in $PKS0745-191$[97], Virgo[98], and possibly A2390[43]. The mini-halo in A2390 is polarized at levels of $10-20\%$.

Gitti et al.[99] suggested that the electrons of the Perseus mini-halo cannot be supplied by the central radio galaxy, but are continuously undergoing reacceleration due to the MHD turbulence associated with the cooling flow region. They show that an isotropic magnetic field compression[100] appears to well reproduce the observed surface brightness profile and total synchrotron spectrum along with the radial spectral steepening. On the other hand the radial compression of the magnetic field[101] does not appear to be applicable to the mini-halo in the Perseus cluster. The above model was successfully applied also to the mini-halo in A2626[102]. Pfrommer and Enßlin[103], on the other hand, discussed the possibility that relativistic electrons in mini-halos are of secondary origin and thus produced from the interaction of cosmic ray protons with the ambient thermal protons.

4.4. *Magnetic fields beyond clusters*

Recent attempts to detect intergalactic magnetic fields beyond clusters, i.e. in even more rarefied regions of the intergalactic space, have shown recent promise in imaging diffuse synchrotron radiation of very low level. A very faint emission has been detected at 327 MHz with the WSRT in the Coma cluster region between the radio halo Coma C and the relic 1253+275[104]. The surface brightness of this diffuse emission is very low and it is only enhanced at low frequency and low resolution, so it is only visible as a positive noise in Fig. 3. The existence of this feature is confirmed by the asymmetric extension of the central halo Coma C imaged at 1.4 GHz with the Effelsberg single dish[35], and by the VLA data at 74 MHz[36]. The equipartition magnetic field in this region[105] is $\simeq 10^{-7}$G. These data may indicate the existence of a more widespread and somewhat lower intergalactic magnetic field than in the ICM. It could be possibly associated with large-scale shocks related to the formation of the large-scale structure in the universe.

A possible evidence of magnetic field in the intergalactic medium is found[106] in the filament of galaxies ZwCl 2341.1+0000 at z $\sim$ 0.3.

The study of the RM of distant quasars could provide an independent information on the magnetic field in the intergalactic medium. An upper limit of $\lesssim 10^{-9}$ G for a cosmic magnetic field outside clusters of galaxies has been derived in the literature[1,107]. However, this limit relies on several assumptions. New generation instruments will shed light on this point.

5. Hard X-Ray Emission in Clusters

Diffuse radio sources are not the only indication of non-thermal activity in the ICM. The prospects for the X-ray detection of inverse-Compton emission originating from radio emitting electrons and photons of the microwave background were presented about 30 years ago[108,109]. Significant progress in the search of non-thermal emission in the hard X-ray band ($>$ 20 keV, HXR) has been recently made owing to

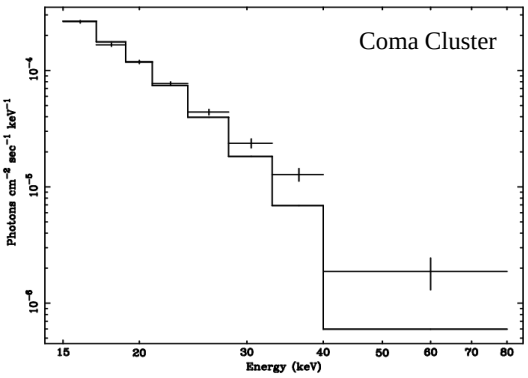


Fig. 5. Coma cluster — PDS data. The continuous line represents the best fit with a thermal component at the average cluster gas temperature of 8.1 keV. The errors bars are quoted at the 1σ level[114].

the improved sensitivity and wide spectral capabilities of the *BeppoSAX* and the *Rossi X-ray Timing Explorer* (RXTE) satellites (see the review by Fusco-Femiano et al.[110]).

Evidence for the presence of HXR radiation in excess to the thermal emission has been obtained in the spectrum of Coma[111,112,113,114]. In Fig. 5, we report the combined hard X–ray spectrum of the Coma cluster, obtained using *BeppoSAX* data of two independent observations of 90 ksec and 300 ksec[114]. The non-thermal excess with respect to the thermal emission is at a confidence level of $\sim 4.8\sigma$ and has a flux of $(1.5 \pm 0.5) \times 10^{-11}$ erg cm^{-2} s^{-1} in the 20–80 keV energy band (assuming a photon index $\Gamma_X = 2.0$). In the framework of the IC model (see Sec. 3.4) the combination of the radio and non-thermal X–ray fluxes allows an estimate of the volume-averaged intracluster magnetic field of ~ 0.2 μG.

In addition to Coma, HXR non-thermal emission has been detected in A2256[115,116]. The flux in the 20 – 80 keV energy range is $\sim 9 \times 10^{-12}$ erg cm^{-2} s^{-1}. A magnetic field of ~ 0.05 μG is derived for the northern cluster region, where the radio relic is located, while a higher field value, ~ 0.5 μG, could be present at the cluster center, in the region of the radio halo. A HXR detection at low confidence level is obtained in A754[117,118], where however a radio galaxy with BL Lac characteristics could be responsible for the emission.

The detection in A2199, which is a cooling core cluster with no extended diffuse radio emission, is controversial[110,119]. A marginal detection has been obtained in A119[110], a merging cluster without a radio halo, but the presence of several point sources in the field of view makes the IC interpretation unlikely.

For the clusters A3667[120] and A2163[38] only upper limits to the non-thermal X-

ray emission have been derived. A possible detection in A2319 with RXTE[121] leads to a magnetic field of $0.1 - 0.3$ μG. Localized IC emission associated with the radio relic and with merger shocks in A85 has been claimed from ROSAT observations[122]. The derived magnetic field is ~ 1 μG.

The value of the magnetic field derived in the Coma cluster by the IC HRX emission is quite consistent with that obtained by the radio halo Coma C under equipartition conditions (Sec. 4.1), but it is much lower than that derived from RM measurements (see next section). Therefore, alternative interpretations to the IC model for the non-thermal radiation detected in the Coma cluster have been proposed. A suggested mechanism is the non-thermal bremsstrahlung from supra-thermal electrons formed through the current acceleration of the thermal gas[123,124,125,126]. However, Petrosian[127] pointed out that due to the low efficiency of the bremsstrahlung mechanism, these models would require an unrealistically high energy input.

We will show in Sec. 9 that the disagreement between IC and RM magnetic field measurements can be at least partially alleviated. Future studies of non-thermal X-ray emission in clusters will be possible with the *ASTRO-E2* satellite.

6. Rotation Measures

One of the key techniques used to obtain information about the cluster magnetic fields strength and geometry is the Faraday rotation analysis of radio sources in the background of clusters or in the galaxy clusters themselves.

RM calculated from extragalactic radio sources can be considered as the sum of three integrals which represent the contribution of three different regions, namely internal to the source itself, due to our own Galaxy, and occurring in the ICM. The latter is the RM in which we are interested here.

Typical values of the RM of Galactic origin are of the order of 10 rad m^{-2} for most sources, and up to $\simeq 300$ rad m^{-2} for sources at low Galactic latitudes[128]. Once the contribution of our Galaxy is subtracted, however, the RM of radio galaxies located inside or behind clusters should be dominated by the contribution of the ICM.

High resolution RM studies of Cygnus A[129] were the first to demonstrate that the high RM values with large gradients on arcsec scales cannot be either of Galactic origin or due to a thermal gas mixed with the radio plasma, but must arise in an external screen of magnetized, ionized plasma. Similarly, the asymmetric depolarization found in double radio lobes embedded in galaxy clusters can be understood as resulting from a difference in the Faraday depth of the two lobes[130,131,132](Laing-Garrington effect). Indeed, the radio source lobe pointing towards the observer is less depolarized than the lobe pointing away.

The observing strategy to get information on the cluster magnetic field intensity and structure is to obtain high resolution RM maps of sources located at different impact parameters of a cluster, then derive the average value of the rotation measure

$\langle \mathrm{RM} \rangle$ and the value of its dispersion σ_{RM}. As described in Sec. 3.5.2, the RM values are combined with measurements of the thermal gas density n_e to estimate the cluster magnetic field along the line of sight. Such studies have been carried out on both statistical samples and on individual objects.

The first successful statistical demonstrations of Faraday rotation from radio sources seen through a cluster atmosphere were presented by Lawler and Dennison[14] for a dozen of radio galaxies and by Vallée et al.[133] for A2319. In both studies, a broadening of the values of RM was found in the cluster sources, with respect to the sources in a control sample.

Kim et al.[33] investigated the magnetic field in the Coma cluster using 18 radio sources, and found a significant enhancement of the RM in the inner parts of the clusters. They deduced a field strength of ~ 2 μG. For the magnetic field structure, they assumed the simple model with a single typical length for field reversal, i.e. a cluster field consisting of cells of uniform size, with the same electron density and magnetic field strength, but with a random field orientation. They obtained a cell size in the range $10 - 30$ kpc. In the following year, Kim et al.[134] improved the statistics by analyzing a much larger sample of 106 radio sources, and deduced that magnetic fields strengths in the cluster gas are of the order of 1 μG. In a more recent statistical study, Clarke et al.[135] analyzed the RMs for a representative sample of 27 cluster sources, plus a control sample, and found a statistically significant broadening of the RM distribution in the cluster sample, and a clear increase in the width of the RM distribution toward smaller impact parameters. Their estimates give a magnetic field of $4 - 8$ μG, assuming a cell size of ~ 15 kpc.

The first detailed studies of RM on individual clusters have been performed in cooling core clusters, owing to the presence of powerful radio galaxies at their centers. Extreme values of RMs are found to be associated with these radiogalaxies, with the magnitude of the RMs roughly proportional to the cooling rate.[136]. Magnetic fields, from ~ 5 μG up to the values of ~ 30 μG are deduced in the innermost regions of these clusters, e.g. Hydra A[137] and 3C295[138,139].

Polarization data from sources at different cluster locations have been obtained in clusters without cooling cores, i.e. Coma[16], A119[140], A514[141], 3C129[142], A400[143], A2634[143]. In the Coma cluster, Feretti et al.[16] derived a magnetic field of 7 μG tangled on scales of ~ 1 kpc, in addition to a weaker field component of ~ 0.2 μG, ordered on a scale of about one cluster core radius. Generally, a decreasing $|\langle \mathrm{RM} \rangle|$ and σ_{RM} with an increasing projected distance from the cluster center is found. RM gradients are detected across the sources, indicating the presence of structure in the intracluster magnetic field. The data lead to magnetic field estimates of $\sim 2 - 8$ μG, with patchy structures of $\sim 5 - 15$ kpc.

Overall, the data are consistent with cluster atmospheres containing μG fields, with perhaps an order of magnitude scatter in field strength between clusters, or within a given cluster, and with extreme field values in cluster cooling cores. These estimates of the magnetic field strength from RM data crucially depend on the

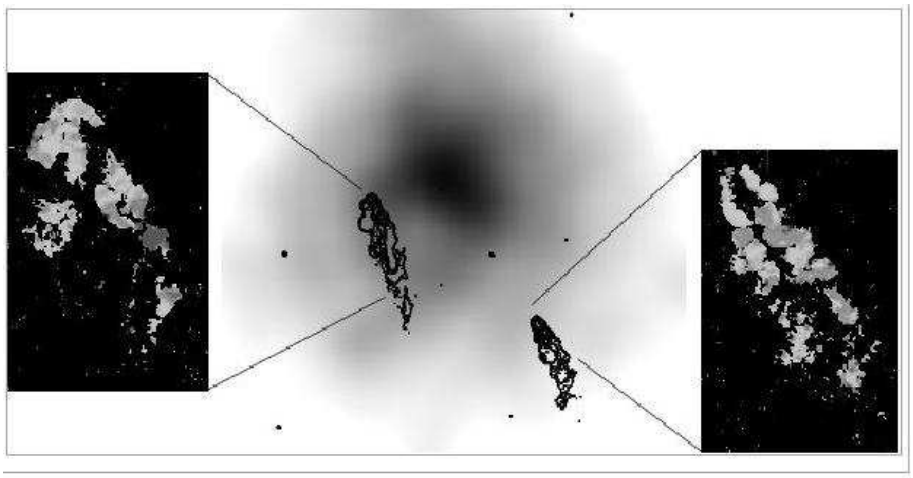


Fig. 6. VLA contour plot at 21 cm and RM images (insets) of the two tailed radio galaxies 0053-015 (left) and 0053-016 (right) in A119[140]. The contour plot is overlaid onto the ROSAT X-ray image (gray-scale) of the cluster. The two radio galaxies are located at a projected distance from the cluster center of $\sim 0.45 r_c$ and $1.2 r_c$ respectively. Both the RM images show fluctuations on small scales ($\sim$ 10 kpc). The RM values in 0053-015 are between -350 rad m^{-2} and $+450$ rad m^{-2} with $\langle \mathrm{RM} \rangle = 28$ rad m^{-2}, and $\sigma_{\mathrm{RM}} = 152$ rad m^{-2}. The RM values in 0053-016 are between -300 rad m^{-2} and $+200$ rad m^{-2}, with $\langle \mathrm{RM} \rangle = -79$ rad m^{-2} and $\sigma_{\mathrm{RM}} = 91$ rad m^{-2}.

magnetic field structure and geometry. The RM distribution is generally patchy, indicating that large-scale magnetic fields are not regularly ordered on cluster scales, but have structures on scales as low as 10 kpc or less. In Fig.6 we show the RM images obtained for the two central radio galaxies in A119[140].

In many cases, high resolution RM images show a nearly Gaussian RM distribution, suggesting an isotropic distribution of the field component along the line-of-sight. However, many RM distributions show clear evidence for a non-zero mean $\langle \mathrm{RM} \rangle$ if averaged over areas comparable with the radio source size, even after the Galactic contribution is subtracted. These $\langle \mathrm{RM} \rangle$ offsets are likely due to fluctuations of the cluster magnetic fields on scales greater than the typical source size, i.e. considerably larger than those responsible for the RM dispersion. The random magnetic field must therefore both be tangled on sufficiently small scales, in order to produce the smallest structures observed in the RM images and also fluctuate on scales one, or even two, orders of magnitude larger, to account for the non-zero RM average. For this reason, it is necessary to consider cluster magnetic field models where both small and large scale structures coexist.

So far very little attention has been given in the literature to the determination of the power spectrum of the intracluster magnetic field fluctuations. Very recently Enßlin and Vogt[144] and Vogt and Enßlin[145] pointed out that the single scale cell model is not realistic because it does not satisfy the condition $\mathbf{div}\vec{B} = 0$. By using a semi-analytic technique, they showed that the magnetic field power spectrum

can be estimated by Fourier transforming RM maps if very detailed RM images are available. Moreover, they derived that the autocorrelation length of the RM fluctuations is in general larger than the magnetic field autocorrelation length.

An alternative numerical approach to investigate the strength and structure of cluster magnetic fields through Monte Carlo simulations is presented in Murgia et al.[146]. A brief description of the capability of such a numerical approach is presented in Sec. 10.

It is worth mentioning here that some authors have suggested the possibility that the RM observed in radio galaxies is not associated with the foreground ICM, but may arise locally to the radio source[147,148], either in a thin skin of dense warm gas mixed along the edge of the radio emitting plasma, or in its immediate surroundings. There are, however, several arguments against this interpretation:
i) the trends of RM versus the cluster impact parameter in both statistical studies and individual cluster investigations,
ii) the relation between the RM and the cooling flow rate in relaxed clusters[136],
iii) the Laing-Garrington effect[130,131,132],
iv) statistical tests on the scatter plot of RM versus polarization angle, for the radio galaxy PKS1246-410 [150],
v) the very consistent scenario drawn by all the results presented in this section.
Thus, we conclude that local effects might give some contribution to the RM, however the major factor responsible for the Faraday Rotation should be the ICM. Future high resolution RM studies with the next generation radio telescopes (e.g. EVLA, LOFAR, SKA) should help in distinguishing the local effects, as well as possible effects arising internally to the radio sources.

7. Cluster Cold Fronts

The high sensitivity and resolution of the *Chandra* satellite has allowed the detection in the clusters A2142 and A3667 of sharp discontinuities in the X-ray surface brightness, the so called cold fronts[151,152,153]. Ettori and Fabian[154] pointed out that the observed temperature jumps in A2142 require that thermal conduction across cold fronts must be suppressed by a factor of 100 or more, compared to the classical Spitzer value[155]. Actually, a tangled magnetic field has been found[156] to reduce the thermal conductivity from the Spitzer value by a factor of order 10^2 - 10^3.

Similar features have now been detected in several other clusters[65,157,158]. These structures are apparently contact discontinuities between the gas which was in the cool core of one of the merging sub-clusters and the surrounding intracluster gas. They are not shocks because the density increase across the front is accompanied by a temperature decrease such that there is no dramatic change in the pressure and entropy.

In the cluster A3667[152,153] (see Fig. 7), the temperature discontinuity in the cold front occurs over a scale of $3.5''(\simeq 4$ kpc). Vikhlinin et al.[153] suggested that in order to reproduce such a sharp feature, magnetic fields are required to suppress

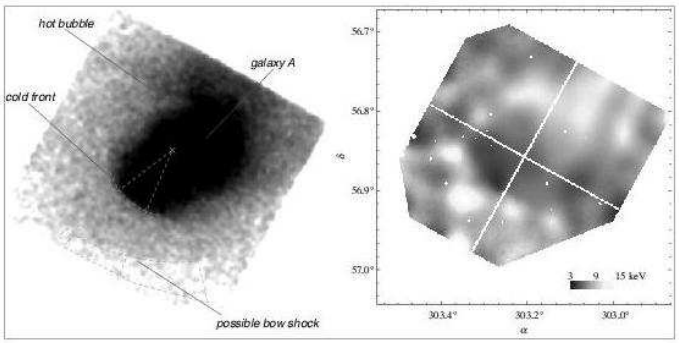


Fig. 7. Chandra X-ray image (left) and temperature map (right) of A3667[152,153].

both thermal conduction and Kelvin-Helmholtz instabilities along the contact discontinuity. They found that the front sharpness and its gradual smearing at large angles are most likely explained by the existence of a layer with a $\simeq 10\ \mu$G magnetic field parallel to the front. The magnetic filed in the layer is probably amplified by the stretching of the field lines.

8. Magnetic Field Profile

The simplest model for a cluster magnetic field is a uniform field through the whole cluster. However, this is not realistic: if the field values detected at the cluster centers would extend over several core radii, up to distances of the order of $\sim$ Mpc, the magnetic pressure would exceed the thermal pressure in the outer parts of the clusters.

Jaffe[159] first suggested that the magnetic field distribution in a cluster would depend on the thermal gas density and on the distribution of massive galaxies and therefore would decline with the cluster radius. Constraints to the radial gradient of the cluster magnetic field strength are provided by observations of clusters hosting a radio halo. Indeed, the spatial correlation found in some clusters between the X-ray cluster brightness and the radio halo brightness[70] implies that the energy densities in the thermal and non-thermal components have a similar radial scaling, thus a magnetic field decline is inferred.

A radial decrease of the cluster magnetic field strength is also deduced in the framework of halo formation models which consider the reacceleration of the radio emitting electrons. The radial steepening of the synchrotron spectrum, observed in Coma[34] and more recently in A665[75] and A2163[75], is interpreted as the result of the combination of the magnetic field profile with the spatial distribution of the reacceleration efficiency, thus allowing us to set constraints on the radial profile of the cluster magnetic field. In Fig. 8 we show the magnetic field profile in the Coma cluster obtained by Brunetti et al.[50] by applying a model for the electron reacceleration. Different lines refer to different values of the reacceleration coefficient. The

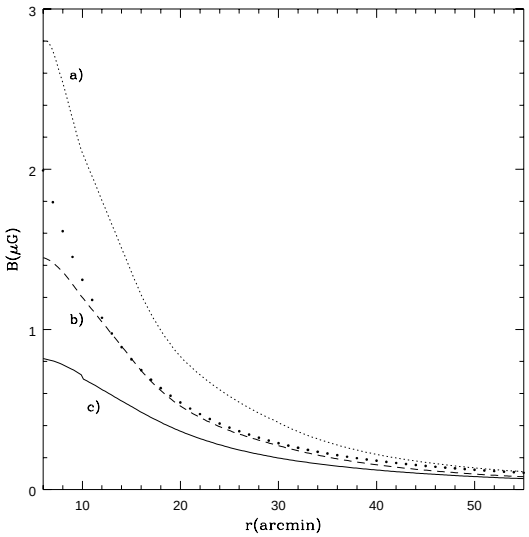


Fig. 8. The magnetic field profile in the Coma cluster obtained from the radial spectral steepening, by applying an electron reacceleration model. The figure is from Brunetti et al.[50], who use $H_0 = 50$ km s^{-1} Mpc^{-1}. The trends, however, do not depend on the assumed cosmology. Different lines refer to different values of the reacceleration coefficient. The dots represents the Jaffe[159] theoretical predictions for the magnetic field distribution in the Coma cluster.

dots represents the Jaffe[159] theoretical prediction. The field intensity is found to decrease smoothly from $\sim\ 0.5 - 1.5\ \mu$G at the cluster center to $\sim\ 0.03 - 0.5\ \mu$G at ~ 1.3 Mpc radius, with a trend similar to that of the thermal gas. The magnetic field profiles in A665[75] and A2163[75] show a flatter decline, probably because the ongoing violent mergers in these clusters are playing a significant role in determining the conditions of the radiating particles and of the magnetic field.

Important clues on the magnetic field distribution are also derived from MHD cosmological simulations. Dolag et al.[160,161] simulated the formation of magnetized galaxy clusters from an initial density perturbation field, using a cosmological MHD code. They found that the μG level field presently observed in clusters can be reproduced by the evolution of the magnetic field starting from an initial field of $\sim 10^{-9}$ G at redshift 15. This field is amplified by compression during the cluster collapse. They obtained that the process of large-scale structure formation in the universe drives the characteristics of these magnetic fields. One of their results is that the magnetic field strength at any point within galaxy clusters is proportional to the gas density.

In the simple case of adiabatic compression during a spherical collapse due to gravity, the field lines are frozen into the plasma, and compression of the plasma results in compression of flux lines. The expected growth of the magnetic field is roughly proportional to the gas density as $B \propto \rho^{2/3}$, as a consequence of magnetic flux conservation.

From the simulations, Dolag et al.[162] predict the existence of a correlation between the Faraday rotation measure and the X-ray flux. They find that σ_{RM} increases with the X-ray flux:

$$\sigma_{RM} \propto S_x^f, \tag{47}$$

with $f \simeq 1$.

The X-ray surface brightness is:

$$S_x \propto \int n_e^2 \sqrt{T}\, dl. \tag{48}$$

The RM dispersion, obtained from Eq. 44, is related to B and n_e. The two observables σ_{RM} and S_x relate the two line of sight integrals with each other, therefore in comparing these two quantities, we actually compare cluster magnetic field versus thermal density. Thus the magnetic field profile can be represented by:

$$B(r) \propto n_e(r)^\eta. \tag{49}$$

In the case of the β-model (Eq. 45), the X-ray flux S_x is:

$$S_x \propto (1 + r_\perp^2/r_c^2)^{-3\beta+\frac{1}{2}}. \tag{50}$$

By substituting Eq. 49 in the expression of σ_{RM} derived from Eq. 44, we obtain:

$$\sigma_{RM} \propto (1 + r_\perp^2/r_c^2)^{-\frac{3}{2}\beta(1+\eta)+\frac{1}{4}} \tag{51}$$

Thus, by comparing S_x and σ_{RM}, one finds that the index η is related to the slope f and to the parameter β, through:

$$\eta = \frac{1}{\beta}(2f - 1)(\beta - \frac{1}{6}) \tag{52}$$

We note that for a constant magnetic field ($\eta = 0$) the slope of the $\sigma_{RM} - S_x$ correlation should be $f = 0.5$ while a steeper slope would imply $\eta > 0$.

For the cluster A119, where the polarization properties of 3 extended radio galaxies are available, the σ_{RM} – S_x relation yields $B \propto n_e^\eta$ with $\eta = 0.9$. This implies that the central magnetic field[162] in this cluster is ≈ 9 μG, instead of the ≈ 6 μG inferred by using the constant magnetic field approximation[140].

The simulations not only predict that the magnetic field scales similarly to the density within all clusters but also that clusters should have different central magnetic field strengths depending on their temperature, and therefore their mass. Indeed, the normalization of the σ_{RM} – S_x relation is expected to be related to the cluster temperature. In Fig. 9, the predicted σ_{RM} – S_x relation at different cluster temperatures has been compared with the observations for a sample of clusters with good RM data.

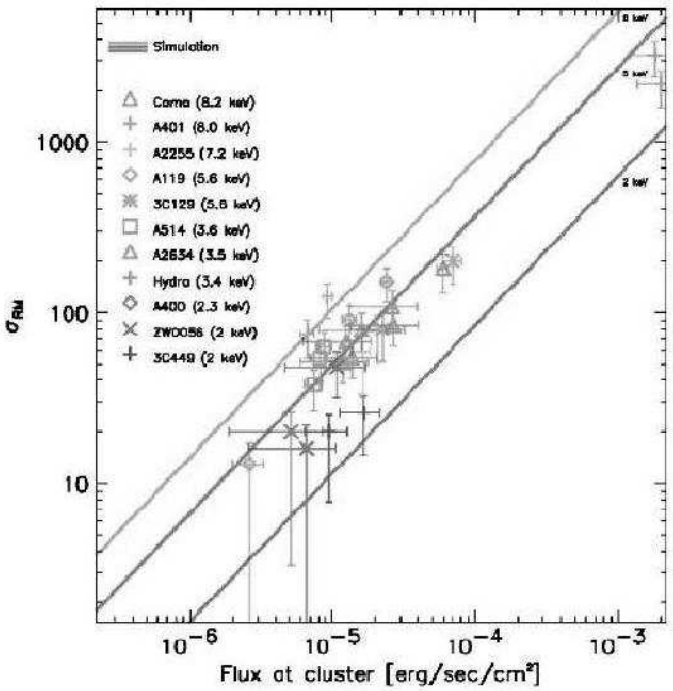


Fig. 9. The correlation between the observed σ_{RM} and the X-Ray flux, and comparison with theoretical predictions (kindly supplied by K. Dolag). The data points are marked with different grey scale levels according to the individual cluster temperature. Theoretical predictions are shown as lines for three temperatures. Data points for different sources in the same cluster follow very well the predicted lines. The simulations also predict these lines to be shifted according to the temperature of the cluster. This trend is also confirmed by the data points.

9. Reconciling Magnetic Field Values

From the results presented in the previous sections, it is derived that cluster magnetic field strengths obtained from RM arguments (Sec. 6) are about an order of magnitude higher than the estimates obtained from both the diffuse synchrotron radio halo emission under equipartition conditions (Sec. 4.1) and the inverse Compton hard X-ray emission (Sec. 5). Relatively high magnetic fields could be present in regions of radio relics at the cluster periphery (Sec. 4.2), and in cold fronts (Sec. 7). However, it is important to note that magnetic field estimates derived in relics and in cold fronts may be not representative of the overall cluster magnetic field strengths because they have been likely enhanced by compression.

The clusters Coma and A3667[86] are unique in that they allow the field to be estimated by using different techniques. Examples of the variation of magnetic field strength estimates from various methods and in various locations of these clusters are given in Table 3.

Several arguments can be invoked to alleviate the discrepancies between different

Table 3. Magnetic field estimates derived from various methods in the clusters Coma and A3667.

Name	Method	Field strength (μG)	Location	Reference
Coma	Equipartition	0.45	radio halo	34
	Equipartition	0.55	radio relic	77
	Faraday Rotation	7	cluster center	16
	Faraday Rotation	0.2	cluster center(large scale)	16
	Inverse Compton	0.2	cluster average	114
A3667	Equipartition	1.5−2.5	NW relic	86
	Inverse Compton	≥ 0.4	cluster average	120
	Faraday Rotation	1−2	cluster center	86
	Faraday Rotation	3−5	NW relic	86
	Cold front	10	along the cold fronts	153

Column 2 gives the method used to estimate the field strength, Column 3 the value of the magnetic field in μG, Column 4 describes the location in the cluster at which this estimation is made, Column 5 gives the reference.

methods of analysis. First, we remind that the equipartition values rely on several assumptions (Sec. 3.2). Moreover, the radio synchrotron and IC emissions originate from large cluster volumes, and the corresponding magnetic field estimates are averaged over the whole cluster, whereas the RM gives an average of the field along the line of sight, weighted by the thermal gas distribution. Taking into account the radial profile of the cluster magnetic field and of the gas density, Goldshmidt and Rephaeli[163] first showed that the field strength estimated with the IC method is expected to be smaller than that measured with the RM observations. Beck et al.[164] pointed out that field estimates derived from RM may be too large in the case of a turbulent medium where small-scale fluctuations in the magnetic field and the electron density are highly correlated. Finally, more realistic electron spectra should be considered in the analysis of synchrotron and IC emission. It has been shown that IC models which include both the expected radial profile of the magnetic field, and anisotropies in the pitch angle distribution for the electrons allow higher values of the ICM magnetic field in better agreement with the Faraday rotation measurements[46,127]. Moreover, as shown in Table 3, the magnetic field strength may vary depending on the dynamical history and the location within the cluster.

In some cases a radio source could compress the gas and fields in the ICM to produce local RM enhancements[147,148] (see also Sec. 6), thus leading to overestimates of the derived ICM magnetic field strength.

The magnetic field may show complex structure, as filaments and/or substructure with a range of coherence scales, therefore the interpretation of RM data as given in Sec. 3.5.2 would be too simplified. Indeed, Newman et al.[149] demonstrated that the assumption of a single-scale magnetic field leads to an overestimation of the magnetic field strength calculated through RM studies. In the next section we show that the use of a numerical approach can significantly improve our interpretation of the data and thus the knowledge of the strength and structure of magnetic fields.

10. Cluster Magnetic Fields Through a Numerical Approach

We have seen that cluster magnetic field strengths can be calculated through their effects on the polarization properties of radio galaxies by using an analytical formulation (Sec. 3.5.2) based on the approximation that the magnetic field is tangled on a single scale. However, detailed observations of radio sources and MHD simulations[144,145,161] suggest that it is necessary to consider more realistic cluster magnetic fields which fluctuate over a wide range of spatial scales. To accomplish this, Murgia et al.[146] simulated random three-dimensional magnetic fields with a power-law power spectrum: $|B_\kappa|^2 \propto \kappa^{-n}$, where κ represents the wave number of the fluctuation scale. They investigated the effects of the expected Faraday rotation on the polarization properties of radio galaxies and radio halos, by analyzing the rotation measure effects produced by a magnetic field with a power spectrum which extends over a large range of spatial scales ($6 - 770$ kpc) and with different values of the spectral index ($n = 2, 3, 4$).

10.1. *Simulated rotation measures*

Fig. 10 (top) shows the simulated RM images obtained with different values of the index n for a typical cluster of galaxies (see caption for more details). Different power spectrum indexes will generate different magnetic field configurations and therefore will give rise to very different simulated RM images. Fig. 10 (bottom) shows the simulated profiles of $\sigma_{\rm RM}$, $|\langle {\rm RM} \rangle|$, and $|\langle {\rm RM} \rangle|/\sigma_{\rm RM}$ (left, central and right panels, respectively), as a function of the projected distance from the cluster center. While both $\sigma_{\rm RM}$ and $|\langle {\rm RM} \rangle|$ increase linearly with the cluster magnetic field strength, the ratio $|\langle {\rm RM} \rangle|/\sigma_{\rm RM}$ depends only on the magnetic field power spectrum slope, for a given range of fluctuation scales. Therefore the comparison between RM data of radio galaxies embedded in a cluster of galaxies and the simulated profiles, allows the inference of both the strength and the power spectrum slope of the cluster magnetic field.

Typical measured values of $|\langle {\rm RM} \rangle|/\sigma_{\rm RM}$ for cluster radio galaxies are derived to be in the range 0.2 - 1.2, once the Galaxy contribution is subtracted[146]. Thus the comparison of the observations with the simulations leads to a rather flat cluster magnetic field power spectrum, with a spectral index $n \simeq 2$. This indicates that most of the magnetic energy density is on the smaller scales.

Another result of the simulations is that, when a power spectrum of the magnetic field is assumed, the inferred magnetic field strength is about a factor of 2 lower than the value computed from Eq. 46 if the single scale Λ_c is taken to be equal to the smallest patchy structures detectable in the RM images, as frequently used. This implies that the magnetic fields derived from RM measurements may be overestimated (see Sec. 9).

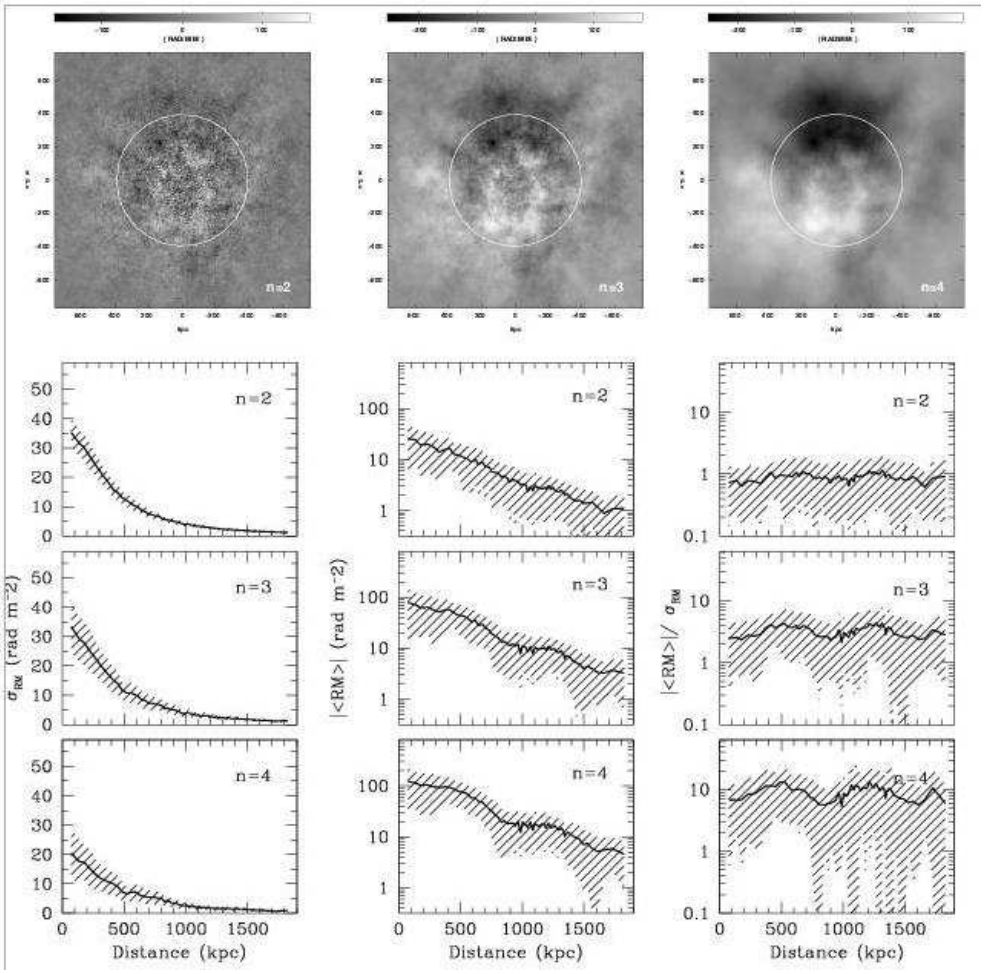


Fig. 10. Top: simulated RM images for magnetic field power spectrum spectral index $n = 2, 3, 4$. The electron gas density of the cluster follow a standard β-model with a core radius $r_c = 400$ kpc (indicated by a circle in the figure) a central density $n_e(0)=10^{-3}$ cm^{-3} and $\beta = 0.6$. The three power spectra are normalized to have the same total magnetic field energy which is distributed over the range of spatial scales from 6 kpc up to 770 kpc. The field at the cluster center is $B_0 = 1$ μG and its energy density decreases from the cluster center according to $B(r)^2 \propto n_e(r)$. Bottom: radial profiles ($\sigma_{\rm RM}$, $|\langle {\rm RM}\rangle|$ and $|\langle {\rm RM}\rangle|/\sigma_{\rm RM}$ respectively) obtained from the RM simulations described above. The profiles have been obtained by averaging the simulated RM images in regions of 50×50 kpc^2, which is a typical size for radio galaxies. The figure is from Murgia et al.[146]

10.2. *Simulated radio halo polarization*

Different values of the power spectrum spectral index will generate very different total intensity and polarization brightness distributions for the radio emission of a halo. So far, polarization emission from radio halos has not been detected. The current upper limits to the polarization at 1.4 GHz are a few percent ($\sim 5\%$).

Murgia et al.[146] simulated the expected halo total intensity and polarization brightness distributions at 1.4 GHz and 327 MHz, as they would appear when observed with a beam of $45''$, by introducing in the 3-dimensional magnetic field an isotropic population of relativistic electrons. Different values of the magnetic field strength and power spectrum index were assumed.

Fig. 11 (top) shows simulated radio halo brightness and polarization percentage distributions at 1.4 GHz (see caption for more details). Fig. 11 (bottom) shows the expected fractional polarization profiles at 1.4 GHz and 327 MHz for the different values of the average magnetic field strength and power spectrum spectral index. Simulations indicate that a power spectrum slope steeper than $n = 3$ and a magnetic field strength lower than $\sim 1\mu$G result in a radio halo polarization percentage at 1.4 GHz far in excess of the current observational upper limits. This means that, in agreement with the RM simulations, either the power spectrum spectral index is flatter than $n = 3$ or the magnetic field strength is significantly higher than $\sim 1\mu$G. The halo depolarization at 327 MHz is particularly severe and the expected polarization percentage at this frequency is always below 1%. Moreover it is also evident that the magnetic field power spectrum slope has a significant effect in shaping the radio halo. In particular, flat power spectrum indexes ($n < 3$) give raise to very smooth radio brightness images (under the assumption that the radiating electrons are uniformly distributed).

11. Origin and Amplification of Cluster Magnetic Fields

The origin of the magnetic fields observed in galaxies and clusters of galaxies is debated. Very little is known about their existence before and after the time of recombination, their evolution, and the possible impact they could have on galaxy and structure formation. We very briefly give the outlines of the main scenarios proposed for the magnetic fields in the ICM, without going into the details, which can be found in the literature[4,5].

According to the first scenario, cluster magnetic fields may be *primordial*, i.e. generated in the early universe prior to recombination[3]. In this case, magnetic fields would be already present at the onset of structure formation, and would be a remnant of the early Universe. One mechanism for the generation of primordial fields involves the "Biermann battery" effect[165], which occurs when the gradients of electron pressure and number density are not parallel, thus electrostatic equilibrium is no longer possible. This leads to a thermoelectric current which generates an electric field (and a corresponding magnetic field) that restores force balance. Other possibilities might be that weak seed fields were formed in the phase transitions of the early Universe, such as a quark-hadron (QCD), or electroweak (EW) transition, where local charge separation occurs creating local currents, or during inflation, where electromagnetic quantum fluctuations are amplified[166]. Values of these seed fields are of the order of $\sim 10^{-21}$ G.

In principle, the presence of magnetic fields in the very early Universe might be

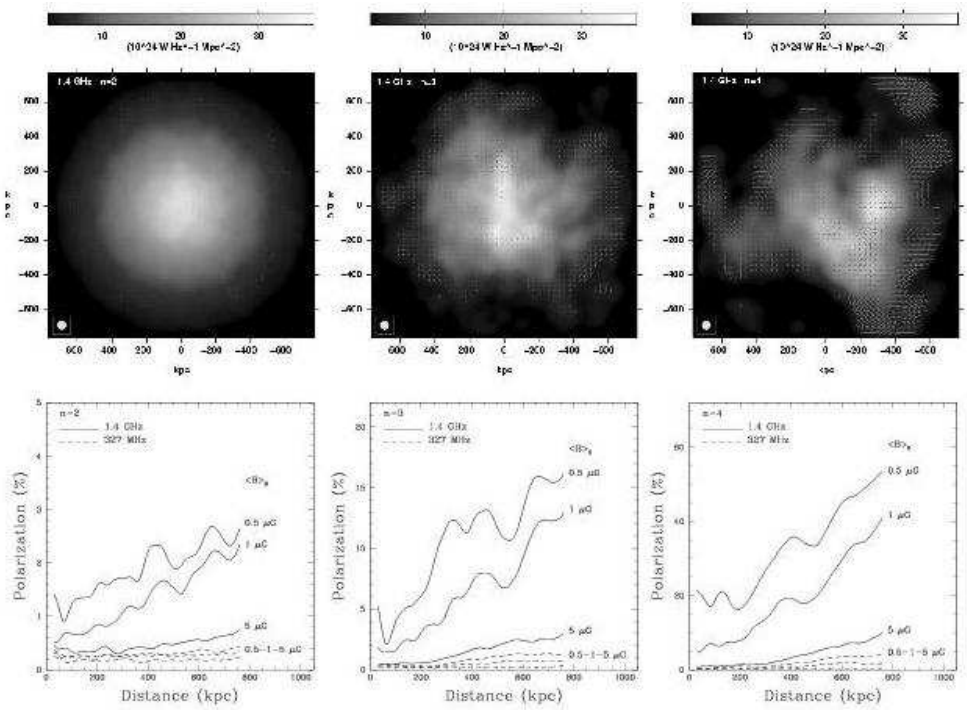


Fig. 11. Simulated halo brightness and polarization degree[146] for cluster at $z = 0.075$ as it would appear when observed with a beam of $45''$. Top: simulated halo images at 1.4 GHz for different values of the magnetic field power spectrum slope n and B_0=1 μG; the vectors lengths are proportional to the degree of polarization, with 100 percent corresponding to 100 kpc on the sky. Field directions are those of the E-vector. Bottom: radially averaged profiles of the polarization percentage at 327 MHz and 1.4 GHz for three values of the magnetic field strength, namely $\langle B \rangle_0 =$ 0.5, 1 and 5 μ G.

detectable through their effect on the Big Bang nucleosynthesis, or if the expansion is observed to be anisotropic. Current observations of anisotropy in the CMB place weak upper limits ($B < 5 \times 10^{-9}$ G) on the strength of a homogeneous component of a primordial magnetic field generated in this way[167]. By analyzing the effect of the inhomogeneities in the matter distribution of the universe on the Faraday rotation of distant QSOs, limits of $B < 10^{-9} - 10^{-8}$ G are obtained[168], depending on the assumed scales of the fluctuations.

Another scenario is that the cosmological magnetic fields are generated in later epochs of the Universe. Gnedin et al.[169] argued that the strongest "Biermann battery" effects are likely to be associated with the epoch of cosmological reionization. Kulsrud et al.[170] investigated the possibility that the field may be *protogalactic*, i.e. generated during the initial stages of the structure formation process, during the protogalaxy formation.

A third scenario involves the *galactic* origin, i.e. ejection from galactic winds of normal galaxies or from active and starburst galaxies[171,172]. Galaxy outflows, gas

stripping, ejection from the AGN by radio jets, all contribute to deposit magnetic fields into the ICM. Galactic fields may be arise from the fields in the earliest stars, then ejected into the interstellar medium by stellar outflows and supernova explosions. Alternatively, fields in galaxies may result directly from a primordial field that is adiabatically compressed when the protogalactic cloud collapses. Indeed, battery mechanism on galactic scales can generate fields up to 10^{-19} G.

Support for a galactic injection in the ICM comes from the evidence that a large fraction of the ICM is of galactic origin, since it contains a significant concentration of metals. However, fields in clusters have strengths and coherence size comparable to, and in some cases larger than, galactic fields[3]. Therefore, it seems quite difficult that the magnetic fields in the ICM derive from ejection of the galactic fields. The recent observations of strong magnetic fields in galaxy clusters suggest that the origin of these fields may indeed be primordial.

The observed field strengths greatly exceed the amplitude of the seed fields, or of fields injected by some mechanism. Therefore, magnetic field amplification seems unavoidable. Dynamo effect can be at work. A magnetic dynamo consists of electrically conducting matter moving in a magnetic field in such a way that the induced currents maintain and amplify the original field[2]. The essential features of the galactic dynamo model are turbulent motions in the interstellar medium, driven by stellar winds, supernova explosions, and hydromagnetic instabilities.

In addition, amplification can occur during the cluster collapse. During the hierarchical cluster formation process, mergers generate shocks, bulk flows and turbulence within the ICM. The first two of these processes can result in some field amplification simply through compression. However, it is the turbulence which is the most promising source of non-linear amplification. MHD calculations have been performed[160,173,174] to investigate the origin, distribution, strength and evolution of the magnetic fields. The results of these simulations show that cluster mergers can dramatically alter the local strength and structure of cluster-wide magnetic fields, with a strong amplification of the magnetic field intensity. The initial field distribution at the beginning of the simulations at high redshift is irrelevant for the final structure of the magnetic field. The final structure is dominated only by the cluster collapse. Fields can be amplified from values of $\sim 10^{-9}$ G to $\sim 10^{-6}$ G.

Roettiger et al.[174] found a significant evolution (see Fig. 12) of the structure and strength of the magnetic fields during two distinct epochs of the merger evolution. In the first, the field becomes quite filamentary as a result of stretching and compression caused by shocks and bulk flows during infall, but only minimal amplification occurs. In the second, amplification of the field occurs more rapidly, particularly in localized regions, as the bulk flow is replaced by turbulent motions. Shear flows are extremely important for the amplification of the magnetic field, while the compression of the gas is of minor importance. Mergers change the local magnetic field strength drastically. But also the structure of the cluster-wide field is influenced. At early stages of the merger the filamentary structures prevail. This structure breaks down later ($\sim$ 2–3 Gyr) and leaves a stochastically ordered magnetic field.

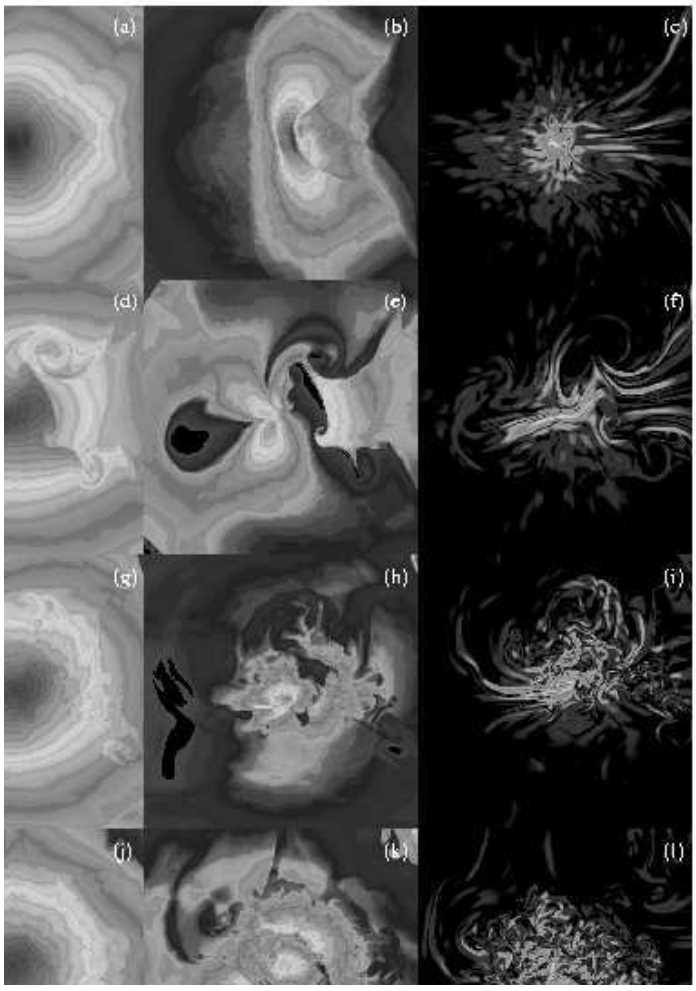


Fig. 12. Three-dimensional numerical MHD simulations of magnetic field evolution in merging clusters of galaxies[174]. The evolution of gas density (column 1), gas temperature (column 2), and magnetic pressure (column 3) in two-dimensional slices taken through the cluster core in the plane of the merger. The four rows represent different epoch during the merger: t = 0,1.3, 3.4, and 5.0 Gyr, respectively.

12. Conclusions

Our knowledge of the magnetic field properties in galaxy clusters has significantly improved in recent years, owing to the improved capabilities of radio and X-ray telescopes. It is well established that μG level magnetic fields are widespread in the

ICM, regardless of the presence of large-scale diffuse radio emission. The magnetic field strengths show almost an order of magnitude scatter between clusters, or within a given cluster, and are extreme in cluster cooling cores. For such large fields the magnetic pressure is comparable to or larger than the gas pressure derived from X-ray data, suggesting that magnetic fields may play a significant role in the cluster dynamics.

The observations are often interpreted in terms of the simplest possible model, i.e. a constant field throughout the whole cluster. However, a decline with radius is expected if the intensity of the magnetic field results from the compression of the thermal plasma during the cluster gravitational collapse. Observational evidence of magnetic field profiles has been derived in some clusters. Moreover the magnetic field could show complex structure with a range of coherence scales.

The study of cluster magnetic fields has gained a big interest in recent years, leading to several new observations as well as simulations. There are, however, still many questions to answer: are the fields filamentary, what are the coherence scales, to what extent do the thermal and non-thermal plasmas mix in cluster atmospheres, how do the fields extend, what is the radial trend of the field strength, how does the field strength depend on cluster parameters such as the gas temperature, metallicity, mass, substructure and density profile, how do the fields evolve with cosmic time, and finally how were the fields generated?

New generation instruments in the radio band, as the EVLA, LOFAR and SKA, are rather promising and will establish a clear connection between radio astronomical techniques and the improvement in the knowledge of the X-ray sky. There are various satellite missions, as *ASTRO-E2*, *XEUS* and *Constellation X*, which will map the X-ray sky at low and high energies in the next years. These will provide a more precise knowledge of the X-ray surface brightness of clusters, i.e. of their thermal gas density, allowing a more accurate and correct interpretation of the sensitive RM measurements. The detection of HXR non-thermal emission will provide independent measurements of the magnetic fields. The accurate experimental determination of large-scale magnetic fields in the intracluster medium will thus be possible. The detection of synchrotron radiation at the lowest possible levels will allow the measurement of magnetic fields in even more rarefied regions of the intergalactic space, and the investigation of the relation between the formation of magnetic fields and the formation of the large-scale structure in the universe.

Acknowledgments

We are grateful to Rainer Beck, Gianfranco Brunetti, Tracy Clarke, Klaus Dolag, Torsten Enßlin, Roberto Fanti, Roberto Fusco-Femiano, Gabriele Giovannini, Dan Harris, Melanie Johnston-Hollitt, Phil Kronberg, Matteo Murgia, Greg Taylor, and Corina Vogt for several fruitful discussions on this topic, and for suggestions. We are indebted to Klaus Dolag for supplying Fig. 9.

References

1. P. P. Kronberg, *Reports of Progress in Physics* **57**, 325 (1994)
2. R. Beck, A. Brandenburg, D. Moss, A. Shukurov, and D. Sokoloff, *ARA&A* **34**, 155 (1996)
3. D. Grasso, and H. R. Rubinstein, *Physics Report* **348**, 163 (2001)
4. C. L. Carilli, and G. B. Taylor, *ARA&A* **40**, 319 (2002)
5. L. M. Widrow, *Reviews of Modern Physics* **74**, 775 (2002)
6. M. Giovannini, *IJMPD* **13**, 391 (2004)
7. B. J. Burn, *MNRAS* **133**, 67 (1966)
8. D. D. Sokoloff, A. A. Bykov, A. Shukurov, E. M. Berkhuijsen, R. Beck, and A. D. Poezd, *MNRAS* **299**, 189 (1998)
9. D. D. Sokoloff, A. A. Bykov, A. Shukurov, E. M. Berkhuijsen, R. Beck, and A. D. Poezd, *MNRAS* **303**, 207 (1999)
10. A. G. Pacholczyk, *Radio Astrophysics*, San Francisco:Freeman (1970)
11. R. Beck, and M. Krause,*A&A*, in preparation (2004)
12. G. Brunetti, G. Setti, and A. Comastri, *A&A* **325**, 898 (1997)
13. G. R. Blumenthal, and R. J. Gould, *Reviews of Modern Physics* **42**, 237 (1970)
14. J. M. Lawler and B. Dennison, *ApJ* **252**, 81 (1982)
15. P. C. Tribble, *MNRAS* **250**, 726 (1991)
16. L. Feretti, D. Dallacasa, G. Giovannini, and A. Tagliani, *A&A* **302**, 680 (1995)
17. J. E. Felten, *In: Clusters, Lensing, and the Future of the Universe*, ASP Conference Series, Vol. 88, Eds. V.Trimble and A.Reisenegger, p. 271, (1996)
18. A. Cavaliere, and R. Fusco-Femiano, *A&A* **49**, 137 (1976)
19. L. Feretti and G. Giovannini, *In: Extragalactic Radio Sources*, IAU Symp. 175, Eds. R. Ekers, C. Fanti, and L. Padrielli, Kluwer Academic Publisher, p. 333 (1996)
20. J. J. Condon, W. D. Cotton, E. W. Greisen, Q. F. Yin, R. A. Perley, G. B. Taylor, and J. J. Broderick, *AJ* **115**, 1693 (1998).
21. G. Giovannini, M. Tordi, and L. Feretti, *New Ast.* **4**, 141 (1999)
22. R. B. Rengelink, Y. Tang, A. G. de Bruyn, G. K. Miley, M. N. Bremer, H. J. A. Roettgering, and M. A. R. Bremer, *A&A Supplement Ser.* **124**, 259 (1997)
23. J.C. Kempner, and C.L. Sarazin, *ApJ* **548**, 639 (2001)
24. D. C. J. Bock, M. I. Large, and E. M. Sadler, *AJ* **117**, 1578 (1999)
25. R. W. Hunstead and the SUMMS team, Proc. Ringberg workshop on *Diffuse Thermal and Relativistic Plasma in Galaxy Clusters*, Eds. H. Böhringer, L. Feretti, and P. Schuecker, MPE report 271, 19 (1999)
26. T. Venturi, S. Bardelli, R. Morganti, and R. W. Hunstead, *MNRAS* **314**, 594 (2000)
27. M. A. G. Willson, *MNRAS* **151**, 1 (1970)
28. W. J. Jaffe, G. Perola, and E. Valentijn , *A&A* **49**, 179 (1976)
29. E. Valentijn, *A&A* **68**, 449 (1978)
30. R. J. Hanisch, T. Matthews, and M. Davis, *A&A* **84**, 946 (1979)
31. R. Schlickeiser, A. Sievers, and H. Thiemann, *A&A* **182**, 21 (1987)
32. P. A. Henning, *AJ* **97**, 1561 (1989)
33. K. T. Kim, P. P. Kronberg, R. E. Dewdney, and T. L. Landecker, *ApJ* **355**, 29 (1990)
34. G. Giovannini, L. Feretti, T. Venturi, K. T. Kim, and P. P. Kronberg, *ApJ* **406**, 399 (1993)
35. B. M. Deiss, W. Reich, H. Lesch, and R. Wielebinski, *A&A* **321**, 55 (1997)
36. T. A. Enßlin, P. P. Kronberg, P. P. Perley, and R. A. Kassim, Proc. Ringberg workshop on *Diffuse Thermal and Relativistic Plasma in Galaxy Clusters*, Eds. H. Böhringer, L. Feretti, and P. Schuecker, MPE report 271, p. 21 (1999)
37. M. Thierbach, U. Klein, and R. Wielebinski, *A&A* **397**, 53 (2003)

38. L. Feretti, R. Fusco-Femiano, G. Giovannini, and F. Govoni, *A&A* **373**, 106 (2001)
39. H. Liang, R. W. Hunstead, M. Birkinshaw, and P. Andreani, *ApJ* **544**, 686 (2000)
40. F. Govoni, L. Feretti, G. Giovannini, H. Böhringer, T. H. Reiprich and M. Murgia, *A&A* **376**, 803 (2001)
41. G. Giovannini and L. Feretti, *New Astronomy* **5**, 335 (2000)
42. T. Venturi, S. Bardelli, D. Dallacasa, G. Brunetti, S. Giacintucci, R. W. Hunstead and R. Morganti, *A&A* **402**, 913 (2003)
43. M. Bacchi, L. Feretti, G. Giovannini and F. Govoni, *A&A* **400**, 465 (2003)
44. T. A. Enßlin, *In: The Universe at Low Radio Frequencies*, IAU Symp. 199, Eds. A. Pramesh Rao, G. Swarup, and Gopal-Krishna (San Francisco: ASP), p. 141 (2002)
45. C. L. Sarazin, 2002, *In: Merging Processes in Galaxy Clusters.* Eds. L. Feretti, I.M. Gioia, and G. Giovannini. Astrophysics and Space Science Library, Vol. 272. Kluwer Academic Publishers, Dordrecht, p. 1
46. G. Brunetti, *In: Matter and Energy in Clusters of Galaxies*, Eds. S. Bowyer, and C.-Y. Hwang, ASP Conf. Ser. 301, (San Francisco: ASP), p. 349 (2003)
47. V. Petrosian, *In: Matter and Energy in Clusters of Galaxies*, Eds. S. Bowyer, and C.-Y. Hwang, ASP Conf. Ser. 301, (San Francisco: ASP), 337 (2003)
48. W. J. Jaffe, *ApJ* **212**, 1 (1977)
49. J. Roland, *A&A* **93**, 407 (1981)
50. G. Brunetti, G. Setti, L. Feretti, and G. Giovannini, *MNRAS* **320**, 365 (2001)
51. H. Ohno, M. Takizawa, and S. Shibata, *ApJ* **577**, 658 (2002)
52. Y. Fujita, M. Takizawa, and C. L. Sarazin, *ApJ* **584**, 190 (2003)
53. C. L. Sarazin, *ApJ* **520**, 529 (1999)
54. Y. Fujita, and C. L. Sarazin, 2001, *ApJ* **563**, 660 (2001)
55. U. Keshet, E. Waxman, and A. Loeb, astro-ph/0402320 (2004)
56. S. Gabici, and P. Blasi, *ApJ* **583**, 695 (2003)
57. D. Ryu, H. Kang, E. Hallman, and T.W. Jones, *ApJ* **593**, 599 (2003)
58. B. Dennison, *ApJ* **239**, L93 (1980)
59. P. Blasi, and S. Colafrancesco, *Astrop. Phys.* **12**, 169 (1999)
60. K. Dolag, and T. A. Enßlin, *A&A* **362**, 151 (2000)
61. L. Feretti, Proc. Ringberg workshop on *Diffuse Thermal and Relativistic Plasma in Galaxy Clusters*, Eds. H. Böhringer, L. Feretti, and P. Schuecker, MPE report 271, p. 3 (1999)
62. D. A. Buote, *ApJ* **553**, L15 (2001)
63. M. Markevitch and A. Vikhlinin, *ApJ* **563**, 95 (2001)
64. M. Markevitch, A. H. Gonzalez, L. David, A. Vikhlinin, S. Murray, W. R. Forman, C. Jones, and W. Tucker, *ApJ* **567**, L27 (2002)
65. M. Markevitch, A. Vikhlinin, and W. R. Forman, *In: Matter and Energy in Clusters of Galaxies*, Eds. S. Bowyer, and C.-Y. Hwang, ASP Conf. Ser. 301, (San Francisco: ASP), p. 37 (2003)
66. M. Markevitch, P. Mazzotta, A. Vikhlinin, D. Burke, et al. *ApJ* **586**, L19 (2003)
67. J. C. Kempner, and L. P. David, *MNRAS* **349**, 385 (2004)
68. F. Govoni, M. Markevitch, A. Vikhlinin, L. VanSpeybroeck, L. Feretti, and G. Giovannini, *ApJ* **605**, 695 (2004)
69. P. Henry, A. Finoguenov, and U. G. Briel, *ApJ* **615**, in press (2004)
70. F. Govoni, T. A. Enßlin, L. Feretti, and G. Giovannini, *A&A* **369**, 441 (2001)
71. G. Giovannini, L. Feretti, and F. Govoni, *In: The Universe at low radio frequencies*, IAU Symp. 199, Eds. Pramesh Rao, G. Swarup, and Gopal-Krisna (San Francisco: ASP), p. 149 (2002)
72. L. Feretti, *In: The Universe at low radio frequencies*, IAU Symp. 199, Eds. Pramesh

Rao, G. Swarup and Gopal-Krisna (San Francisco: ASP), p. 133 (2002)
73. S. Colafrancesco, Proc. Ringberg workshop on *Diffuse Thermal and Relativistic Plasma in Galaxy Clusters*, Eds. H. Böhringer, L. Feretti, and P. Schuecker, MPE report 271, p. 269 (1999)
74. D. E. Harris, V. K. Kapahi, and R. D. Ekers, *A&AS* **39**, 215 (1980)
75. L. Feretti, E. Orrú, G. Brunetti, G. Giovannini, N. Kassim, and G. Setti, *A&A* in press, astro-ph/0404283 (2004)
76. B. Ballarati, L. Feretti, A. Ficarra, G. Giovannini, M. Nanni, M. C. Olori, and G. Gavazzi, *A&A* **100**, 323 (1981)
77. G. Giovannini, L. Feretti, L. and C. Stanghellini, *A&A* **252**, 528 (1991)
78. A. H. Bridle, and E. B. Fomalont, *A&A* **52**, 107 (1976)
79. H. J. A. Röttgering, I. Snellen, G. Miley, J. P. de Jong, R. J. Hanisch, and R. Perley, *ApJ*, **436**, 654 (1994)
80. T. E. Clarke, and T. A. Ensslin, *In: Clusters of Galaxies and the High Redshift Universe Observed in X-rays*, Eds. D.M. Neumann, and J.T.T. Van., http://www-dapnia.cea.fr/Conferences/Morion_astro_2001/index.html, (2001)
81. J. O. Burns, K. Roettiger, J. Pinkney, R. A. Perley, F. O. Owen, and W. Voges, *ApJ* **446**, 583 (1995)
82. L. Feretti, H. Böhringer, G. Giovannini, and D. Neumann, *A&A* **317**, 432 (1997)
83. A. D. Reid, R. W. Hunstead, L. Lemonon, and M. M. Pierre, *MNRAS* **302**, 571 (1999)
84. N. E. Kassim, T. E. Clarke, T. A. Enßlin, A. S. Cohen, and D. M. Neumann, *ApJ* **559**, 785 (2001)
85. H. J. A. Röttgering, M. H. Wieringa, R. W. Hunstead, and R. D. Ekers, *MNRAS* **290**, 577 (1997)
86. M. Johnston-Hollitt , *In: The Riddle of Cooling Flows in Galaxies and Clusters of Galaxies*, Eds. T, H. Reiprich, J.C. Kempner, and N. Soker, http://www.astro.virginia.edu/coolflow/, (2003)
87. D. E. Harris, C. P. Stern, A. G. Willis, and P. E. Dewdney, *AJ* **105**, 769 (1993),
88. T. A. Enßlin, P. L. Biermann, U. Klein, and S. Kohle *A&A* **332**, 395 (1998)
89. K. Roettiger, J. O. Burns, and J. M. Stone, *ApJ* **518**, 603 (1999)
90. F. Miniati, T. W. Jones, H. Kang, and D. Ryu,*ApJ* **562**, 233 (2001)
91. T. A. Enßlin, and M. Brüggen, *MNRAS* **331**, 1011 (2002)
92. T. A. Enßlin, and Gopal-Krishna *A&A* **366**, 26 (2001)
93. O. B. Slee, A. L. Roy, M. Murgia, H. Andernach, and M. Ehle, *AJ* **122**, 1172 (2001)
94. L. G. Sijbring, PhD Thesis, Groningen University (1993)
95. J. O. Burns, M. E. Sulkanen, G. R. Gisler, and R. A. Perley, *ApJ* **388**, L49 (1992)
96. M. A. Brentjens, and A. G. de Bruyn, *In: The Riddle of Cooling Flows in Galaxies and Clusters of Galaxies*, Eds. T. H. Reiprich, J.C. Kempner, and N. Soker, available electronically at http://www.astro.virginia.edu/coolflow/, (2003)
97. S. A. Baum, and C. P. O'Dea C.P., *MNRAS* **250**, 737 (1991)
98. F. N. Owen, J. A. Eilek, and N. E. Kassim, *ApJ* **543**, 611 (2000)
99. M. Gitti, G. Brunetti, and G. Setti, *A&A* **386**, 456 (2002)
100. P. C. Tribble, *MNRAS* **263**, 31 (1993)
101. N. Soker, and C. L. Sarazin, *ApJ* **348**, 73 (1990)
102. M. Gitti, G. Brunetti, L. Feretti, and G. Setti, *A&A* **417**, 1 (2004)
103. C. Pfrommer, and T. A. Enßlin, *A&A* **413**, 17 (2004)
104. K. T. Kim, P. P. Kronberg, G. Giovannini, and T. Venturi, *Nature* **341**, 720 (1989)
105. P. P. Kronberg, *In: Matter and Energy in Clusters of Galaxies*, Eds. S. Bowyer, and C.-Y. Hwang, ASP Conf. Ser. 301, (San Francisco: ASP), p. 169 (2003)
106. J. Bagchi, T. A. Enßlin, F. Miniati, C. S. Stalin, M. Singh, S. Raychaudhury, and N.

B. Humeshkar, *New Astronomy* **7**, 249 (2002)
107. J. P. Vallée, *ApJ* **360**, 1 (1990)
108. D.E. Harris, and J.E. Grindlay, *MNRAS* **188**, 25 (1979)
109. Y. Rephaeli, *ApJ* **227**, 364 (1979)
110. R. Fusco-Femiano, D. Dal Fiume, M. Orlandini, S. De Grandi, S. Molendi, L. Feretti, P. Grandi, and G. Giovannini, *In: Matter and Energy in Clusters of Galaxies*, Eds. S. Bowyer and C.Y. Hwang, ASP Conf. Ser. 301, p. 109, (2003)
111. R. Fusco-Femiano, D. Dal Fiume, L. Feretti, G. Giovannini, P. Grandi, G. Matt, S. Molendi, and A. Santangelo, *ApJ* **513**, L21 (1999)
112. Y. Rephaeli, D. Gruber, and P. Blanco, *ApJ* **511**, L21 (1999)
113. Y. Rephaeli, and D. Gruber, *ApJ* **579**, 587 (2002)
114. R.Fusco-Femiano, M. Orlandini, G. Brunetti, L. Feretti, G. Giovannini, P. Grandi, and G. Setti, *ApJ* **602**, L73 (2004)
115. R. Fusco-Femiano, D. Dal Fiume, S. De Grandi, L. Feretti, G. Giovannini, P. Grandi, A. Malizia, G. Matt, and S. Molendi, *ApJ* **534**, L7 (2000)
116. Y. Rephaeli, and D. Gruber, *ApJ* **595**, 137 (2003)
117. A. Valinia, M. J. Henriksen, M. Loewenstein, K. Roettiger, R. F. Mushotzky, and G. Madejski, *ApJ* **515**, 42 (1999)
118. R. Fusco-Femiano, M. Orlandini, S. De Grandi, S. Molendi, L. Feretti, G. Giovannini, M. Bacchi, and F. Govoni, *A&A* **398**, 441 (2003)
119. J. S. Kaastra, R. Lieu, J. P. D. Mittaz, J. A. M. Bleeker, R. Mewe, S. Colafrancesco, and F. J. Lockman, *ApJ* **519**, L119 (1999)
120. R. Fusco-Femiano, D. Dal Fiume, M. Orlandini, G. Brunetti, L. Feretti, and G. Giovannini, *ApJ* **552**, L97 (2001)
121. D. Gruber, and Y. Rephaeli, *ApJ* **565**, 877 (2002)
122. J. Bagchi, V. Pislar, and G. B. Lima Neto, *MNRAS* **296**, L23 (1998)
123. T. A. Enßlin, R. Lieu R., and P. L. Biermann, *A&A* **344**, 409 (1999)
124. V. A. Dogiel, *A&A* **357**, 66 (2000)
125. C. L. Sarazin, and J. C. Kempner,*ApJ* **533**, 73 (2000)
126. P. Blasi, *ApJ* **532**, L9 (2000)
127. V. Petrosian, *ApJ* **557**, 560 (2001)
128. M. Simard-Normandin, P. P. Kronberg, and S. Button, *ApJS* **45**, 97 (1981)
129. J. W. Dreher, C. L. Carilli, and R. A. Perley, *ApJ* **316**, 611 (1987)
130. R. A. Laing, *Nature* **331**, 149 (1988)
131. S. T. Garrington, J. P. Leahy, R. G. Conway, and R. A. Laing, *Nature* **331**, 147 (1988)
132. S. T. Garrington, and R. G. Conway, *MNRAS* **250**, 198 (1991)
133. J. P. Vallée, M. J. MacLeod, and N. W. Broten, *A&A* **156**, 386 (1986)
134. K. T. Kim, P. C. Tribble, and P. P. Kronberg, *ApJ* **379**, 80 (1991)
135. T. E. Clarke, P. P. Kronberg, and H. Böhringer, *ApJ* **547**, L111 (2001)
136. G. B. Taylor, A. C. Fabian, and S. W. Allen, *MNRAS* **334**, 769 (2002)
137. G. B. Taylor, and R. A. Perley, *ApJ* **416**, 554 (1993)
138. R. A. Perley, and G. B. Taylor, *AJ* **101**, 1623 (1991)
139. S. W. Allen, G. B. Taylor, P. E. J. Nulsen, R. M. Johnstone, et al., *MNRAS* **324**, 842 (2001)
140. L. Feretti, D. Dallacasa, F. Govoni, G. Giovannini, G. B. Taylor, and U. Klein, *A&A* **344**, 472 (1999)
141. F. Govoni, G. B. Taylor, D. Dallacasa, L. Feretti, and G. Giovannini, *A&A* **379**, 807 (2001)
142. G. B. Taylor, F. Govoni, S. W. Allen, and A. C. Fabian, *MNRAS* **326**, 2 (2001)

143. J. A. Eilek, and F. N. Owen, *ApJ* **567**, 202 (2002)
144. T. A. Enßlin, and C. Vogt, *A&A* **401**, 835 (2003)
145. C. Vogt, and T. A. Enßlin, *A&A* **412**, 373 (2003)
146. M Murgia, F Govoni, L. Feretti, G. Giovannini, D. Dallacasa, R. Fanti, G. B. Taylor, and K. Dolag, *A&A*, in press, astro-ph/0406225 (2004)
147. G. V. Bicknell, R. A. Cameron, and R. A. Gingold, *ApJ* **357**, 373 (1990)
148. L. Rudnick, and K. M. Blundell, *ApJ* **588**, 143 (2003)
149. W. I. Newman, A.L. Newman, and Y. Rephaeli, *ApJ* **575**, 755 (2002)
150. T. A. Ensslin, C. Vogt, T. E. Clarke, and G. B. Taylor, *ApJ* **597**, 870 (2003)
151. M. Markevitch, T. J. Ponman, and P. E. J. Nulsen, et al. *ApJ* **541**, 542 (2000)
152. A. Vikhlinin, M. Markevitch, M., and S. S. Murray, *ApJ* **551**, 160 (2001)
153. A. Vikhlinin, M. Markevitch, M., and S. S. Murray, *ApJ* **549**, L47 (2001)
154. S. Ettori and A. C. Fabian, *MNRAS* **317**, L57 (2000)
155. L. Spitzer, *Fully Ionized Gases*, New York: Interscience (2nd edition), (1962)
156. B. D. G. Chandran, and S. C. Cowley, *Physical Review Letters* **80**, 3077 (1998)
157. M. Sun, S. S. Murray, M. Markevitch, and A. Vikhlinin, *ApJ* **565**, 867 (2002)
158. J. C. Kempner, C. L. Sarazin, and P. M. Ricker, *ApJ* **579**, 236 (2002)
159. W. Jaffe, *ApJ* **241**, 925 (1980)
160. K. Dolag, M. Bartelmann, and H. Lesch, *A&A* **348**, 351 (1999)
161. K. Dolag, M. Bartelmann, and H. Lesch, *A&A* **387**, 383 (2002)
162. K. Dolag, S. Schindler, F. Govoni, and L. Feretti, *A&A* **378**, 777 (2001)
163. O. Goldshmidt, and Y. Rephaeli, *ApJ* **411**, 518 (1993)
164. R. Beck, A. Shukurov, D. Sokoloff and R. Wielebinski, *A&A* **411**, 99 (2003)
165. L. Biermann, *Z. Naturforsch. Tiel A.* 5, 65 (1950)
166. J. M. Stone, *In: Highlights of Astronomy*, Vol. 12, XXIVth General Assembly of the IAU 2000. Ed. H. Rickman. San Francisco, CA: Astronomical Society of the Pacific, p. 709 (2002)
167. J. D. Barrow, P. G. Ferreira, and J. Silk, *Physical Review Letters* **78**, 3610 (1997)
168. P. Blasi, S. Burles, and A. V. Olinto, *ApJ* **514**, L79 (1999)
169. N. Y.Gnedin, A. Ferrara, and E. G. Zweibel, *ApJ* **539**, 505 (2000)
170. R. M. Kulsrud, R. Cen, J. P. Ostriker, and D. Ryu, 1997, *ApJ* **480**, 481 (1997)
171. P. P. Kronberg, H. Lesch, and U. Hopp, *ApJ* **511**, 56 (1999)
172. H. J. Völk, and A. M. Atoyan,*Astrop. Phys.* **11**, 73 (1999)
173. S. Schindler, 2002, *In Merging Processes in Galaxy Clusters*, Eds. L. Feretti, I.M. Gioia, and G. Giovannini, Astrophysics and Space Science Library, Vol. 272. Kluwer Academic Publishers, Dordrecht, p. 229
174. K. Roettiger, J. M. Stone, and J. O. Burns, *ApJ* **518**, 594 (1999)